2023

Ovarian inflammation mediated by Toll-like receptor 4 increased transcripts of maternal effect genes and decreased embryo development

Alison F. Ermisch

Katie L. Bidne

Scott G. Kurz

Kerri A. Bochantin

Jennifer R. Wood

Ovarian inflammation mediated by Toll-like receptor 4 increased transcripts of maternal effect genes and decreased embryo development

Alison F. Ermisch, Katie L. Bidne, Scott G. Kurz, Kerri A. Bochantin and Jennifer R. Wood

Department of Animal Science, University of Nebraska–Lincoln, Lincoln, NE, USA

Correspondence — J.R. Wood, Department of Animal Science, University of Nebraska-Lincoln, 3940 Fair St., Lincoln, NE 68583-0908, USA. Tel: +14024726437; *email* jwood5@unl.edu

Abstract

Obese women are subfertile and have reduced assisted reproduction success, which may be due to reduced oocyte competence. We hypothesize that consumption of a high-fat/high-sugar diet induces ovarian inflammation, which is a primary contributor to decreased oocyte quality and pre-implantation embryo development. To test this hypothesis, C57BL/6 (B6) mice with a normal inflammatory response and C3H/HeJ (C3H) mice with a dampened inflammatory response due to dysfunctional Toll-like receptor 4 were fed either normal chow or high-fat/high-sugar diet. In both B6 and C3H females, high-fat/high-sugar diet induced excessive adiposity and hyperglycemia compared to normal chow-fed counterparts. Conversely, ovarian

Published in *Biology of Reproduction*, 2023, 108(3), pp. 423–436.
doi:10.1093/biolre/ioac212

Submitted May 23, 2022; revised November 3, 2022; accepted November 25, 2022; published 3 December 2022.
Presented in part at the 53rd (St. Louis, MO) Annual Meeting of the Society for the Study of Reproduction.

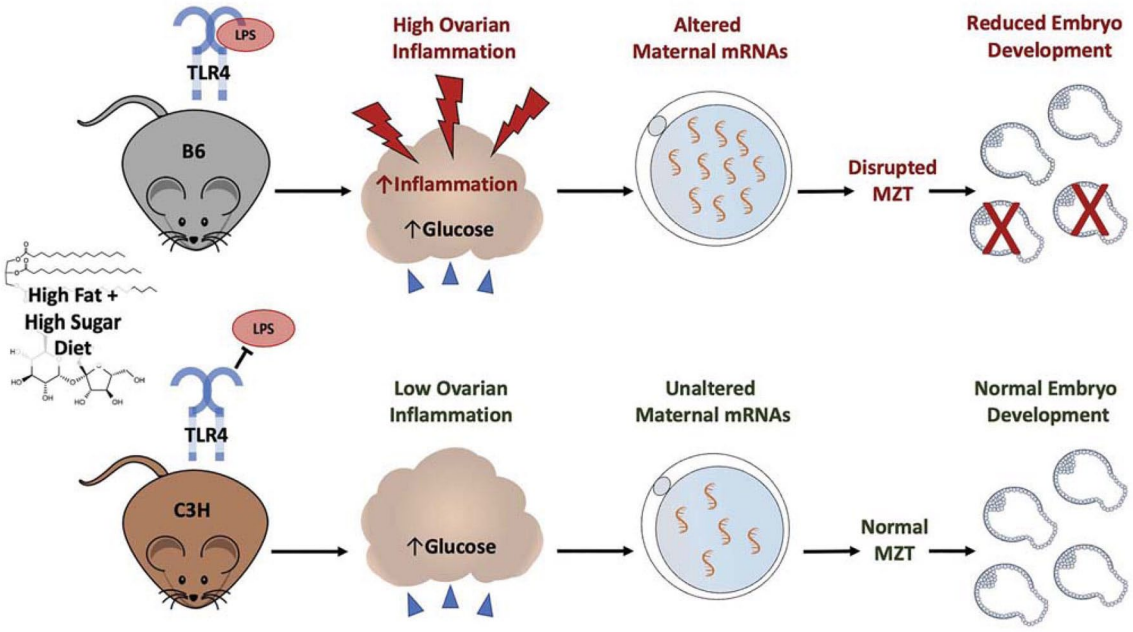

CD68 levels and oocyte expression of oxidative stress markers were increased when collected from B6 high-fat/ high-sugar but not C3H high-fat/high-sugar mice. Following in vitro fertilization of in vivo matured oocytes, blastocyst development was decreased in B6-high-fat/high-sugar but not C3H high-fat/high-sugar mice. Expression of cumulus cell markers of oocyte quality were altered in both B6 high-fat/ high-sugar and C3H high-fat/high-sugar. However, there were no diet-dependent differences in spindle abnormalities in either B6 or C3H mice, suggesting potential defects in cytoplasmic maturation. Indeed, there were significant increases in the abundance of maternal effect gene mRNAs in oocytes from only B6 high-fat/ high-sugar mice. These differentially expressed genes encode proteins of the subcortical maternal complex and associated with mRNA metabolism and epigenetic modifications. These genes regulate maternal mRNA degradation at oocyte maturation, mRNA clearance at the zygotic genome activation, and methylation of imprinted genes suggesting a mechanism by which inflammation induced oxidative stress impairs embryo development.

Keywords: subcortical maternal cortex, RNA binding proteins, oocyte maturation, maternal effect genes, epigenetic regulators, obesity, inflammation

Summary: Ovarian inflammation, due to consumption of a high-fat/high-sugar diet, but not metabolic dysfunction alone, increased mRNA abundance of maternal effect genes in mature oocytes and decreased blastocyst development.

Introduction

Maternal obesity and infertility are intimately linked, with nearly 40% of reproductive aged women classified as obese in the United States [1] and a predicted prevalence of infertility in the general population as high as 18% [2]. Women who are overweight (body mass index 25.0–29.9) or obese (>30) account for roughly 40% of all in vitro fertilization (IVF) procedures [3]. Furthermore, overweight and obese women have lower implantation and clinical pregnancy rates, increased miscarriage rates, and increased risk for premature birth compared to normal weight women [4– 6]. Previous studies have demonstrated that maternal obesity due to consumption of a high fat/high sugar diet leads to a myriad of abnormalities in oocyte growth and maturation, which contribute to both infertility and IVF failure [7–12].

One consequence of maternal obesity is a state of chronic inflammation [13–15]. This phenotype is due in part to increased visceral adipose tissue which produces proinflammatory adipokines and cytokines that contribute to the development of insulin resistance and hyperglycemia [16, 17]. The end result is a state of chronic systemic inflammation and metabolic dysfunction. There are also obesity-induced changes in the gut microbiota that lead to increased gut permeability and subsequent leak of lipopolysaccharide (LPS) into systemic circulation [18]. LPS binds to Toll-like receptor 4 (TLR4), which is recognized as one of the key inducers of the obesity inflammatory response [19]. At the level of tissues and cells, systemic inflammation stimulates proinflammatory cytokine production and induces oxidative stress [13]. It has been well documented that both proinflammatory cytokines and oxidative stress impair oocyte quality [9, 20–23]. Furthermore, recent studies have demonstrated altered meiotic progression and mRNA levels in bovine oocytes following cumulus-oocyte complex (COC) exposure to LPS [24–26].

We previously demonstrated that the abundance of candidate mRNAs were increased in presumptive MII oocytes from mice fed a high fat diet compared to a normal rodent chow diet [27, 28]. These data were consistent with microarray analysis of oocytes from polycystic ovary syndrome (PCOS) patients compared with metabolically normal women, showing that 80% of the differentially expressed genes in PCOS oocytes had increased abundance [29]. The abundance of a

specific mRNA is determined by the sum of its synthesis (transcription) and degradation which occurs in the absence or presence of translation [30]. In the oocyte, transcriptional activity is high during the growth phase [31] followed by transcriptional quiescence as the oocyte approaches ovulation [32]. Furthermore, the abundance of mRNAs and their rate of translation are primarily regulated by post-transcriptional mechanisms. For example, during oocyte growth, many of the mRNAs are bound by Y-box binding protein 2 (MSY2) resulting in highly stable mRNA and low translation rates [33]. Upon luteinizing hormone-induced meiotic resumption mRNA is released from MSY2 and there are transcript-specific changes in each transcripts association with stabilizing or destabilizing RNA-binding proteins (RBPs), the translational machinery, and/or RNA degradation machinery [34]. A subset of the mRNAs, i.e., maternal effect genes, remain stable after ovulation and are translated after fertilization [35]. Maternal effect genes are essential for early embryonic development due to their involvement in transcriptional and cell cycle regulation, epigenetic reprogramming, and other critical processes during the maternal to zygotic transition (MZT) [36]. The importance of maternal effect gene expression and appropriately timed protein translation is evident by the fact that knockout of a single maternal effect gene has no effect on oocyte growth and maturation but causes early embryonic lethality [37–42].

The objective of the current study was to discriminate between the effects of metabolic dysfunction and inflammation on oocyte quality. To achieve this objective, we used two strains of mice, C57BL/6 and C3H/HeJ fed normal rodent chow (ND) or a high-fat/high-sugar (HFHS) diet. Importantly, the C3H/HeJ mice have a spontaneous missense mutation in the *Tlr4* gene, which results in TLR4 protein that is unable to signal upon binding to endotoxins, including LPS and resulting in a dampened inflammatory response [43]. By contrast, the commonly used C57BL/6J mice have a functional TLR4 and diet-induced obesity elicits an innate immune response [44]. By implementing an experimental design utilizing these two mouse models, we identified TLR4 inflammation-dependent decreases in embryo development and increased abundance of maternal effect gene transcripts in response to HFHS-induced obesity.

Materials and methods

Experimental animals and diets

Inbred C57BL6/6 J (B6) and C3H/HeJ (C3H) female mice (The Jackson Laboratory, Bar Harbor, ME) were used for this study. Animals were maintained on a 12:12 light: dark cycle at 25°C with ad libitum access to food and water for the duration of the study. All animal experiments were approved by the University of Nebraska-Lincoln Institutional Animal Care and Use Committee.

Pubertal mice (10-week-old B6 and 8-week-old C3H) were randomly assigned to normal diet (ND; Teklad Global 18% Protein Rodent Diet, Envigo, Indianapolis, IN) or a HFHS diet comprised 42% kcal fat, 42% kcal sucrose (TD.88137, Envigo). In addition to ad libitum access to water, mice in the HFHS experimental group had ad libitum access to 20% sucrose solution (Thermo Fisher Scientific, Waltham, MA) that contained vitamins (0.2% w/v; MP Biomedicals, Irvine, CA) and minerals (0.7% w/v; MP Biomedicals) as described [45]. After 4 weeks on diet (≥25% body weight gain in HFHS diet treatment group), all mice were stimulated with 5 IU pregnant mare serum gonadotropin (PMSG; ProSpec, Rehovot, Israel), followed by 5 IU human chorionic gonadotropin (hCG; Calbiochem EMD Millipore, Billerica, MA) 48 h later. Mice were fasted 12 h prior to euthanasia.

Females were euthanized by isoflurane (MWI Animal Health, Boise, ID) overdose followed by cervical dislocation 16 h after hCG stimulation. Final body weight, percentage body fat and fasting glucose levels were recorded for all females. Fasting blood glucose levels were obtained via glucometer (Contour, Parsippany, NJ) reading of tail tip blood, and percent body fat was determined utilizing the Lunar PIXImus2 Densitometer (General Electric, Boston, MA) to perform DEXA scans. Data were generated from two independent trials with 5–7 female mice per experimental group in each trial.

Cumulus cell and oocyte collection

Following superovulation, cumulus–oocyte masses were removed from the ampulla of the oviduct in warm MOPS-buffered collection medium (oMOPS). Cumulus cells were denuded from oocytes using

a low concentration (50 μg/ml) of hyaluronidase. All oocytes were quickly removed and washed with oMOPS, then cumulus cells were pipetted into a microcentrifuge tube containing cold PBS+0.01% polyvinyl pyrrolidone (PVP). Cumulus cells collected from each female were pelleted individually via centrifugation at 500 RCF for 5 min at 4°C. Excess PBS+PVP was removed, and RNA was immediately extracted from the resulting pellet using TriReagent (Invitrogen) according to the manufacturer's instructions. Oocytes from mice were pooled in groups of 20 (from 1–2 mice), washed thoroughly through drops of PBS+PVP, and immediately subjected to RNA extraction as described above. A subset of oocytes was fixed with 4% paraformaldehyde (PFA) in PBS for spindle staining.

Oocyte spindle staining

To identify abnormalities in spindle morphology, in vivo matured oocytes from B6-ND (n=18), B6-HFHS (n=28), C3H-ND (n=36), and C3H-HFHS (n=31) females were stained and analyzed as previously described [46]. Briefly, denuded oocytes were fixed in 4% PFA for 20 min, washed in PBS with 0.1% Triton X-100 (TX100) and 0.1% PVP, permeabilized in PBS with 1.0% TX100, then blocked for 30 min in PBS with 0.1% TX100, 0.1 M glycine, and 0.5% bovine serum albumin (BSA). Oocytes were incubated overnight at 4°C in a 1:400 dilution of monoclonal anti-tubulin FITC-conjugated antibody (Sigma). Following antibody incubation, oocytes were washed again in PBS+0.1% TX100 and mounted on a glass slide with ProLong Gold Antifade Mountant with DAPI (Invitrogen, Carlsbad, CA). Slides were imaged with a Nikon A1R-Ti2 confocal microscope imaging system. Spindle and chromosomal alignment were considered normal when a barrel-shaped structure was formed by the microtubules and chromosomes were aligned in a compact metaphase plate [47]. Any disruption of microtubule or chromosome arrangement was considered abnormal.

In vitro fertilization and embryo culture

Spermatozoa were collected from the vas deferens and cauda epididymis of a 3-month-old B6D2F1 male (The Jackson Laboratory, Bar Harbor, ME) and capacitated in fertilization medium (mOFM) for 1

h [48]. Oviducts from females (n=5 per treatment) were collected in oMOPS supplemented with 10% fetal calf serum (HyClone Laboratories, Logan, UT). In vivo matured cumulus–oocyte complexes were placed into 50 μL drops of mOFM containing capacitated sperm (1 x 106 sperm/ml) under oil (Spectrum Chemical, New Brunswick, NJ). Gametes were co-incubated for 6 h at 37° C in 6.0% CO_2 and 5.0% O_2. Following IVF, zygotes (B6-ND n=103, B6-HFHS n=94, C3H-ND n=85, C3H-HFHS n=71) were washed and moved into 20 μL drops of step one Optimized Embryo Culture (OEC1) medium [49] supplemented with 8% fatty acid free BSA and cultured in the same conditions. After 48 h in culture, embryos were transferred to 20 μL drops of step two OEC (OEC2) [49]. Blastocyst development was assessed at 96 h (day 4) and blastocyst hatching at 112 h (day 5) of culture.

Blastocyst cell number and allocation

For quantification of inner cell mass (ICM) and trophectoderm (TE) cells, day 5 hatching or fully hatched blastocysts (B6-ND n=31, B6-HFHS n=28, C3H-ND n=21, C3HHFHS n=29) were fixed in 4% PFA and stained as previously described [50, 51]. Briefly, blastocysts were permeabilized in 0.3% Triton X-100 and blocked in a solution containing 0.1% Tween 20, 1.0% BSA, 0.1 M glycine, and 10% Normal Goat Serum. Antibodies against SRY (sex determining region Y)-box 2 (SOX2; Biogenex, Fremont, CA, rabbit monoclonal) and Caudal-type homeobox protein 2 (CDX2; Biogenex, mouse monoclonal) were used to identify ICM and TE cells, respectively. The secondary antibodies Alexa Fluor 555 goat anti-rabbit IgG and Alexa Fluor 488 goat antimouse IgG (Invitrogen, Thermo Fisher Scientific) were used for SOX2 and CDX2, respectively. Blastocysts were mounted using ProLong Gold Antifade Mountant with DAPI. Images were obtained using a Nikon A1R-Ti2 confocal microscope at 40x magnification and cells were counted using FIJI (ImageJ). Total cell number was calculated as the number of SOX2 positive cells plus the number of CDX2 positive cells.

Western blotting

Protein extracts were collected from one whole ovary from each female, as previously described [28]. Ovaries were homogenized in

radioimmunoprecipitation assay buffer containing Halt Protease inhibitor cocktail (Thermo Fisher Scientific). Protein concentration was determined using a bicinchoninic acid assay according to the manufacturer's directions (Thermo Fisher Scientific). Equal amounts of protein (10 μg) per sample (B6-ND, n=11; B6-HFHS, n=13; C3H-ND, n=9; and C3H-HFHS, n=8) were loaded onto 10% SDS-PAGE gels, then transferred to polyvinylidene fluoride membranes (EMD Millipore, Burlington, MA), and blocked with 5% nonfat milk in TBS-T (20 mM Tris–HCl, 15 0 mM NaCl, 0.1% Tween 20, pH 7.3). Membranes were incubated overnight at 4°C in 5% BSA in TBS-T containing primary antibody anti-CD68 (Cluster of differentiation 68; 1:10,000; Cell Signaling Technology, Danvers, MA), followed by incubation with 5% nonfat milk in TBS-T containing anti-rabbit IgG horseradish peroxidase-conjugated secondary antibody (1:20,000; Cell Signaling Technology). To detect protein, blots were incubated with SuperSignal West Femto Maximum Sensitivity Substrate (Thermo Fisher Scientific) and exposed to X-ray film (Research Products International, Prospect, IL). Blots were stripped using Restore Western Blot Stripping Buffer (Thermo Fisher Scientific) and subjected to the same protocol, probed with antibodies for loading control beta-actin (ACTB; 1:20,000). Quantification was performed as previously described [52]. Briefly, protein band intensity was determined for each sample using FIJI, which was then normalized to intensity of ACTB and fold-change between experimental groups was calculated.

Quantitative polymerase chain reaction

RNA from in vivo matured oocytes (20 oocytes per sample; B6-ND n=13, B6-HFHS n=11, C3H-ND n=12, C3HHFHS n=11) and cumulus cells (B6-ND n=10, B6-HFHS n=10, C3H-ND n=11, C3H-HFHS n=11) were reverse transcribed using the iScript Advanced cDNA Synthesis Kit which contains both poly(A) and random primers (Bio-Rad, Hercules, CA) following the manufacturer's instructions. For oocytes, forward and reverse primers for selected maternal effect genes and RBPs (Supplementary Table S1) were designed using NCBI Primer-Blast and synthesized by Integrative DNA Technologies (IDT, Coralville, IA). cDNA was diluted 1:5, and each 10 μL polymerase chain reaction (PCR) reaction included 1 μL cDNA or standard, 300 nM primer mix (forward

and reverse) and 5 μL SsoAdvanced Universal SYBR Green Supermix (Bio-Rad), run in triplicate for each sample. A standard curve for each PCR primer set was generated using gBlock synthetic DNAs which were designed based on amplicon sequence for each gene and synthesized by IDT (Supplementary Table S2). Counts for each sample were interpolated and normalized to H2A.Z variant histone 1 (*H2az1*) [53, 54]. For cumulus cells, primers were designed for markers of oocyte quality (Supplementary Table S1) and quantitative PCR (qPCR) was performed and analyzed in the same manner as oocytes, with 1:5 dilutions of cDNA and transcript counts normalized to *Actb*. In both cell types, the effect of diet (fold-change) was calculated within each mouse line as previously described [55].

Statistics

Statistical analyses were carried out using GraphPad Prism 9 (GraphPad Software, La Jolla, CA). Continuous data (oocytes/female, qPCR, Western blot) with normality of residuals were analyzed using unpaired t-test, whereas data without normality of residuals was analyzed using Mann–Whitney nonparametric test. Continuous data were presented as mean±SEM. Noncontinuous data (embryo stage, degenerate vs. normal oocytes, normal vs. abnormal spindle) were presented as % normal/abnormal. Differences between experimental groups were calculated using Fisher's exact tests. For all statistical analyses, differences were considered significant at $P<0.05$.

Results

HFHS diet induced similar metabolic phenotypes in B6 and C3H females

To determine whether B6 and C3H mice develop similar metabolic phenotypes after consumption of a HFHS diet, pubertal females from each strain were placed on ND or HFHS diet for 4 weeks at which time, all mice fed HFHS had at least a 25% increase in body weight (Supplementary Figure S1). At the end of the trial period, B6 females receiving HFHS diet were significantly ($P<0.0001$) heavier than those on

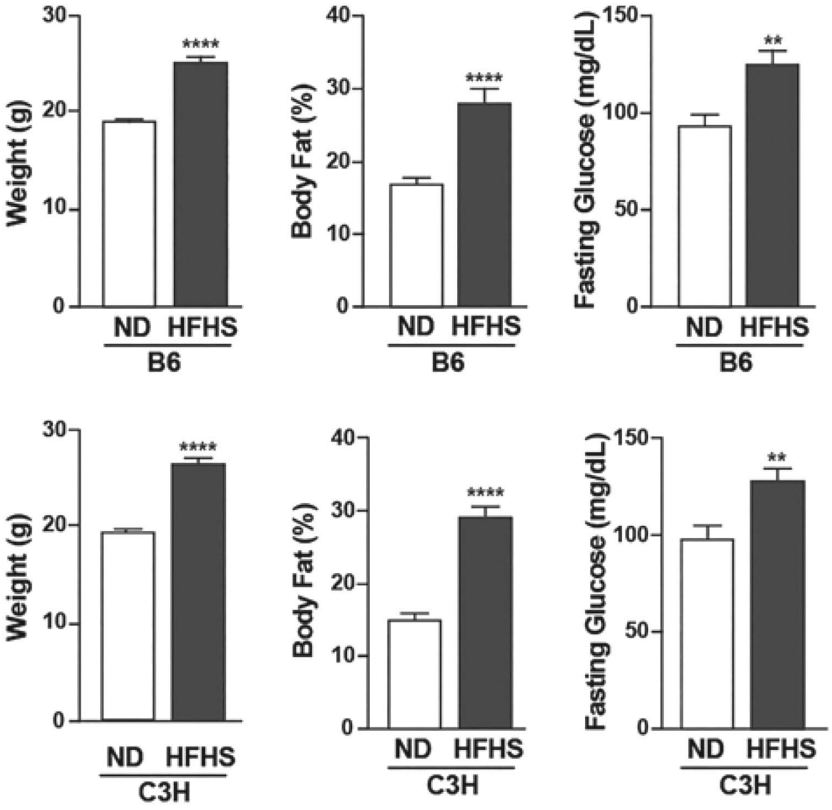

Figure 1. Metabolic phenotypes of C57BL/6 (B6) and C3H/HeJ (C3H) mice. B6 and C3H mice were fed control (ND; white bars) and high fat/high sugar (HFHS; black bars) diet (B6-ND n=9, B6-HFHS n=9, C3H-ND n=8, C3H-HFHS n=8). Final body weight, percent body fat, and fasting glucose levels after 4 weeks on diet were measured. All data are mean±SEM. ***P* <0.01, *****P* <0.0001.

ND (24.6±0.8 g, 19.2±0.2 g, respectively), with B6-HFHS females having a greater body fat percentage than B6-ND females (28.0±1.8%, 16.9±0.6%, respectively) (**Figure 1**). Similarly, C3H females on HFHS diet had a higher final body weight than those on ND (27.4±0.8 g, 19.0±0.3 g, respectively) and greater percent body fat (29.1±1.2%, 15.1±0.7%, respectively). Fasting serum blood glucose levels were higher ($P<0.01$) in B6- HFHS females compared to B6-ND (125.4±6.6 mg/dL, 93.9±5.6 mg/dL, respectively), as well as C3H-HFHS compared to C3H-ND (127.9±6.1 mg/dL, 97.9±6.9, respectively) (Figure 1) indicating that females from both strains acquired similar metabolic phenotypes after consumption of an HFHS diet.

Markers of activated macrophages and oxidative stress were increased in B6-HFHS but not C3H-HFHS ovaries and oocytes

The changes in metabolic phenotypes detected in the HFHS fed mice typically lead to low-level systemic inflammation. Thus, we assessed evidence of the ovarian inflammation by measuring abundance of CD68, a marker of activated macrophages [56]. CD68 was increased 1.6-fold ($P<0.02$) in ovaries from B6-HFHS compared to B6-ND (**Figure 2**A). Conversely, consumption of HFHS diet by C3H mice did not increase CD68 abundance compared to their ND counterparts. Activated macrophages synthesize and secrete proinflammatory cytokines which increase intracellular reactive oxygen species production resulting in oxidative stress [57, 58]. The consequence of oxidative stress is increased expression of antioxidant enzymes including superoxide dismutase 1 (*Sod1*) and glutathione peroxidase (*Gpx1*) [59, 60]. Therefore, we performed real-time qPCR to measure the abundance of *Sod1* and *Gpx1* in oocytes collected from each experimental group. Both *Sod1* and *Gpx1* were increased 2– to 3-fold in oocytes from B6-HFHS compared to B6-ND mice (Figure 2B). However, there was no difference in either transcript in oocytes from C3H-HFHS compared to C3H-ND mice. We also measured the abundance of sirtuin 1 (*Sirt1*), which is a histone deacetylase that contributes to metabolic homeostasis [61]. There was no diet-dependent difference in *Sirt1* mRNA abundance in oocytes from either mouse line. These data demonstrated that B6 females had an expected inflammatory response including oocyte oxidative stress due to HFHS diet consumption. Furthermore, the lack of increased ovarian CD68 and oocyte expression of *Sod1* and *Gpx* in C3H-HFHS versus C3H-ND mice confirmed that the TLR4 mutation resulted in a blunted ovarian inflammatory response.

HFHS diet reduced B6 but not C3H blastocyst development

Based on the phenotypes of B6 and C3H mice, we utilized the two mouse strains to parse out inflammatory versus metabolic effects on oocyte quality and subsequent embryo development. Following IVF there was no difference in the percentage of cleaved embryos derived from oocytes collected from B6-ND (65%) and B6-HFHS (76%) or C3HND (72%) and C3H-HFHS (77%) females (Figure 3A).

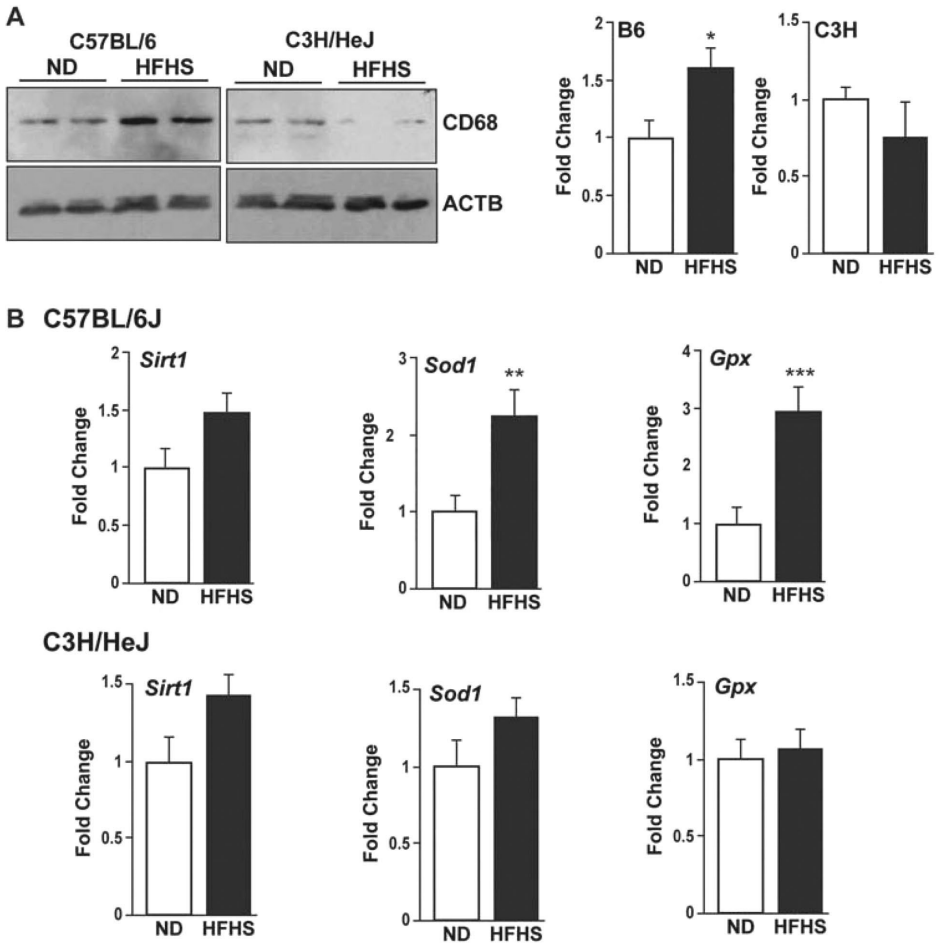

Figure 2. Markers of inflammation and oxidative stress in ovaries and oocytes from C57BL/6 (B6) and C3H/HeJ (C3H) mice. (A) Representative Western blot image and fold change of activated macrophage marker CD68 (cluster of differentiation 68) in ovaries from B6 and C3H females fed normal (ND; white bars) and high fat/high sugar (HFHS; black bars) diet (B6-ND n=11, B6-HFHS n=13, C3H-ND n=9, C3H-HFHS n=8). ACTB, beta-actin. Data are mean±SEM. **P* <0.05. (B) Quantitative, real-time PCR was performed using oocyte mRNA from B6 and C3H females fed normal (ND; white bars) and high fat/high sugar (HFHS; black bars) diet (B6-ND n=11, B6-HFHS n=9, C3H-ND n=11, C3H-HFHS n=9) and primers against *Sirt1* (sirtuin 1), *Sod1* (superoxide dismutase), or *Gpx1* (glutathione peroxidase 1). Data are mean±SEM. ***P* <0.01, ****P* <0.001.

Development from cleaved embryo to day 4 (96 h) blastocysts was decreased (*P*=0.035) in the B6-HFHS group (54%) compared to B6-ND (72%) group. Likewise, development to day 5 (112 h) hatching blastocyst tended to be decreased (*P*=0.060) in the B6-HFHS (38%)

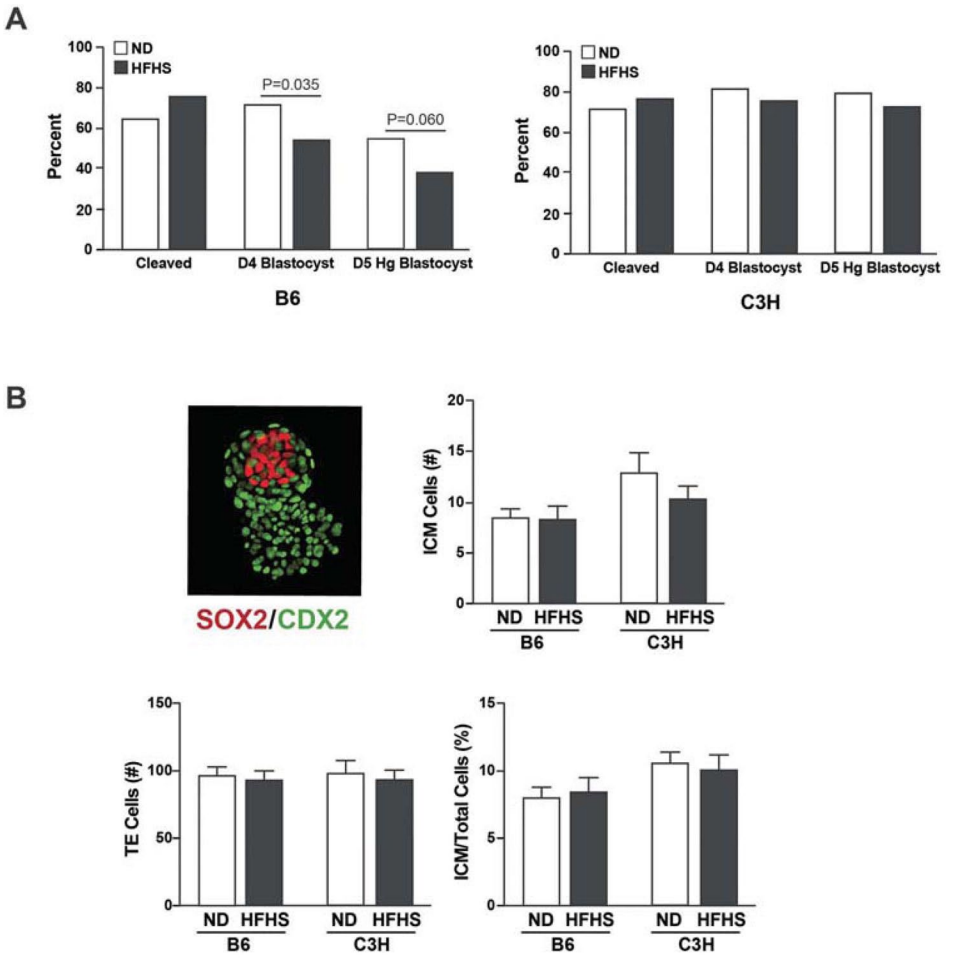

Figure 3. Embryo development rates and blastocyst cell allocation. (A) In vivo matured oocytes from each experimental group were in vitro fertilized and embryos in vitro cultured. The average percent of zygotes that cleaved and developed to blastocyst on day 4 (per cleaved embryo) and hatching blastocyst on day 5 (per cleaved embryo) B6 (B6-ND, B6-HFHS n=94) and C3H (C3H-ND n=85, C3H-HFHS n=71) was calculated. Significant differences (P <0.05) were determined using Fisher exact test. (B) Representative image of a day 5 hatching blastocyst (from C3H-ND) differentially stained for inner cell mass (ICM) cells containing SRY (sex determining region Y)-box 2 (SOX2; red) and trophectoderm (TE) cells containing caudal-type homeobox protein 2 (CDX2; green). Average number of ICM and TE cells and percentage of ICM cells in individual hatching and fully hatched blastocysts (B6-ND n=31, B6-HFHS n=28, C3H-ND n=21, C3H-HFHS n=29) were calculated. Data are mean±SEM.

compared to B6-ND (55%) group (**Figure 3**A). Conversely, there was no difference in blastocyst or hatching blastocyst development after fertilization of oocytes from C3H-ND (82%, 80%) and C3HHFHS (73%,

73%) mice (Figure 3A). To identify any differences in blastocyst morphology between the experimental groups, immunofluorescence of day 5 embryos (hatching or hatched blastocysts) was performed using SOX2 and CDX2 antibodies which stain the ICM and TE, respectively. There was no difference in the number of ICM or TE cells or the ratio of ICM to TE cells per hatched embryo between B6- ND and B6-HFHS or between C3H-ND and C3H-HFHS mice (Figure 3B). Thus, embryos that reached the blastocyst stage, regardless of experimental group, were morphologically normal. However, this does not rule out abnormalities at the cellular level.

Cumulus cell markers of oocyte quality are altered by inflammation and hyperglycemia

To determine if the diet-induced decreases in B6 but not C3H embryo development were due to reduced oocyte quality, we first measured the expression of cumulus cell genes (*Has2, Ptgs2, Ptx3, and Tnfaip6*) that are commonly used markers of oocyte quality (**Figure 4**) [62]. The expression of *Ptx3* and *Tnfaip6* were both decreased in cumulus cells from B6-HFHS compared to B6-ND mice. However, there was no difference in *Has2* or *Ptsg2*. Consumption of HFHS diet by C3H females resulted in decreased expression of not only *Ptx3* and *Tnfaip6* but also *Ptgs2* and *Has2* mRNAs compared to their ND counterparts. Thus, in contrast to the embryo development results, these data suggest reduced quality of the oocytes from both HFHS-fed B6 and C3H mice.

Oocyte meiotic maturation is not altered by HFHS diet

Based on the cumulus gene expression data, we hypothesized that there would be abnormalities in nuclear and/or cytoplasmic maturation in oocytes from mice fed HFHS diet. We first measured common oocyte morphology parameters. After superovulation, there was no diet-dependent difference in the number of in vivo matured oocytes collected per mouse (**Figure 5**A) from B6 (ND=17.4±1.9, HFHS=22.4±3.0) or C3H (ND=22.4±2.4, HFHS=17.8±2.5) females. The number of degenerated oocytes in each experimental group, which was defined as oocytes with pale or fragmented cytoplasm [27], was counted. There was a higher percentage of degenerated oocytes from

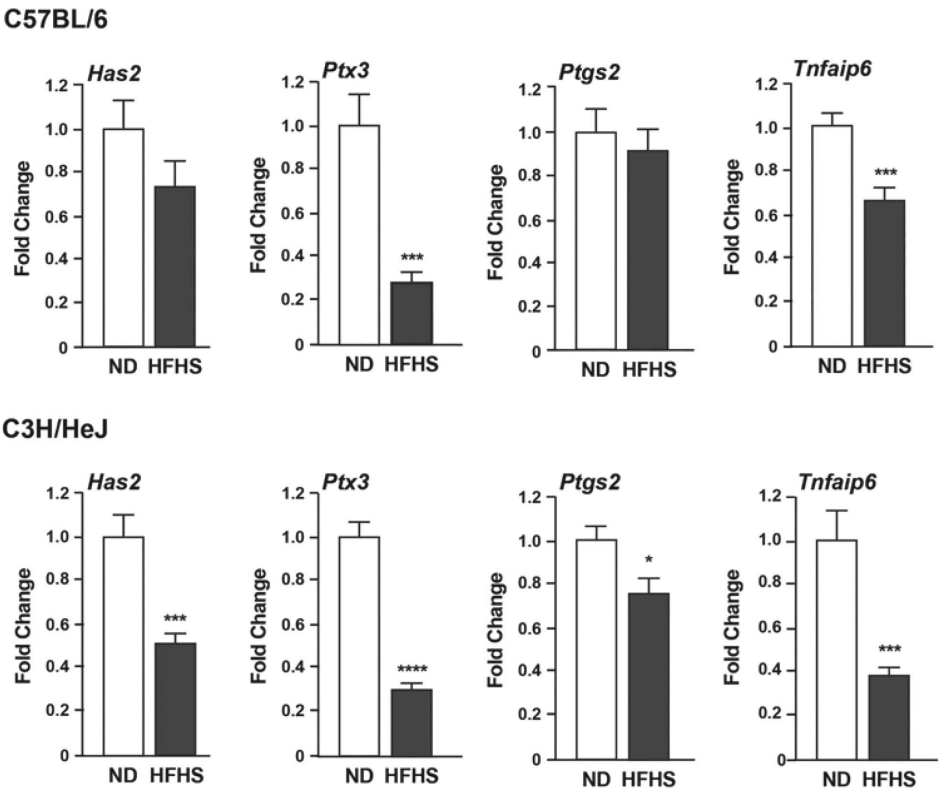

Figure 4. Cumulus cell gene expression. Expression of genes indicative of oocyte quality within cumulus cells from B6 and C3H mice fed control (ND; white bars) and high fat/high sugar (HFHS; black bars) diet (B6-ND n=10, B6-HFHS n=10, C3H-ND n=11, C3H-HFHS n=11). *Has2*, hyaluronan synthase 2; *Ptgs2*, prostaglandin-endoperoxide synthase 2; *Ptx3*, pentraxin 3; *Tnfaip6*, TNF alpha induced protein 6. All data are mean±SEM. **P* <0.05, ****P* <0.001, *****P* <0.0001.

B6-HFHS compared to B6-ND mice but no difference between C3H-ND and C3H-HFHS mice (Figure 5A). Oocytes were subsequently stained with α-tubulin and DAPI to identify any meiotic maturation defects. There were no diet-dependent differences in spindle structure abnormalities or chromosome alignment defects in oocytes from either B6 or C3H mice (Figure 5B).

Maternal effect gene mRNAs were increased in oocytes from B6-HFHS but not C3H-HFHS mice

We previously identified increased abundance of mRNAs, including maternal effect genes, in oocytes from B6 mice fed a 45% high fat

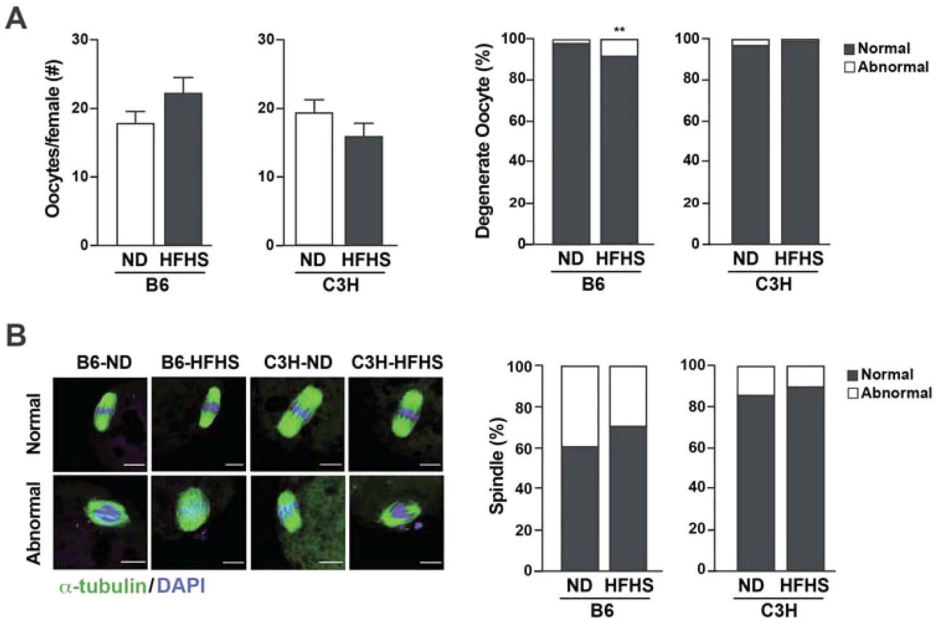

Figure 5. Oocyte morphology. (A) Number of oocytes (mean±SEM) and percent of degenerate oocytes ovulated per B6 and C3H female fed a normal (ND; white bars) or high fat/high sugar (HFHS; black bars) diet (B6-ND n=14, B6-HFHS n=14, C3H-ND n=13, C3H-HFHS n=13). P <0.01 (Fisher's exact test) (B) Representative images stained with α-tubulin (green) and DAPI (blue) and percent of spindle abnormalities in oocytes from B6-ND (n=18), B6-HFHS (n=28), C3H-ND (n=36), and C3H-HFHS (n=31) females. Scale bar=10 μm.

diet [27, 28]. Importantly, these increases were correlated with increased ovarian inflammation and reduced embryonic development. Thus, given the absence of meiotic defects, we next assayed the abundance of maternal effect gene and mRNA metabolism transcripts [36] in oocytes from B6 and C3H mice fed ND or HFHS diet using real-time qPCR. There was increased abundances of transcripts that encode subcortical maternal complex (SCMC) proteins (*Ooep*, *Tle6*, *Nlrp5*, and *Padi6*), a deubiquitinating enzyme (*Uchl1*), RBPs (*Zfp36l2* and *Elavl1*), epigenetic modifiers/chromatin remodelers (*Dnmt1*, *Smarca4* (aka, *Brg1*), *Zfp57* and *Dppa3*), and transcription factors (*Bnc1*, *Pou5f1*, *Sebox*, *Nobox*, and *Figla*) in oocytes from B6-HFHS compared to B6-ND (**Figure 6** & **Figure 7**). However, there were no differences in the abundance of any of these same transcripts between C3H-ND and C3H-HFHS indicating that the diet-dependent increases in oocyte mRNAs in B6 mice was a consequence of ovarian inflammation and/or oocyte oxidative stress.

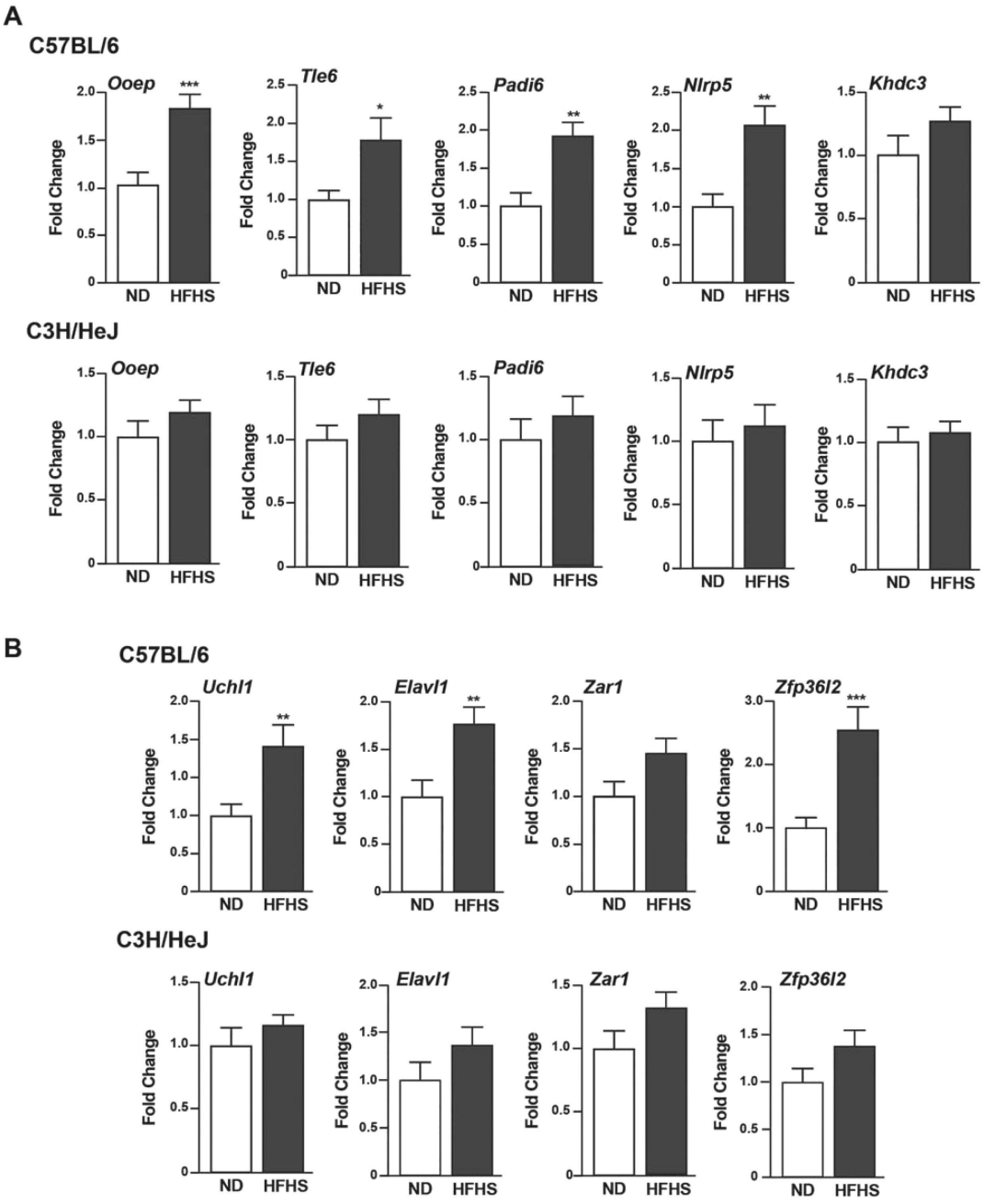

Figure 6. Oocyte gene expression of SCMC and RNA binding proteins. Quantitative, real-time PCR analysis was performed using mRNA from oocytes from B6 and C3H mice fed control (ND; white bars) and high fat/high sugar (HFHS; black bars) diet (20 oocytes per sample; B6-ND n=11, B6-HFHS n=9, C3H-ND n=11, C3H-HFHS n=9) and primers against (A) subcortical maternal complex (SCMC) mRNAs and (B) RNA metabolism factors. Ooep, oocyte expressed protein; Tle6, TLE family member 6; Padi6, peptidyl arginine deiminase 6; Nlrp5, NLR family pyrin domain containing 5; Khdc3, KH domain containing 3; Uchl1, ubiquitin C-terminal hydrolase L1; Elavl1, embryonic lethal abnormal vision like 1; Zar1, zygote arrest 1; Zfp36l2, ZFP36 ring finger protein like 2. All data are mean±SEM. **P* <0.05, ***P* <0.01, ****P* <0.001.

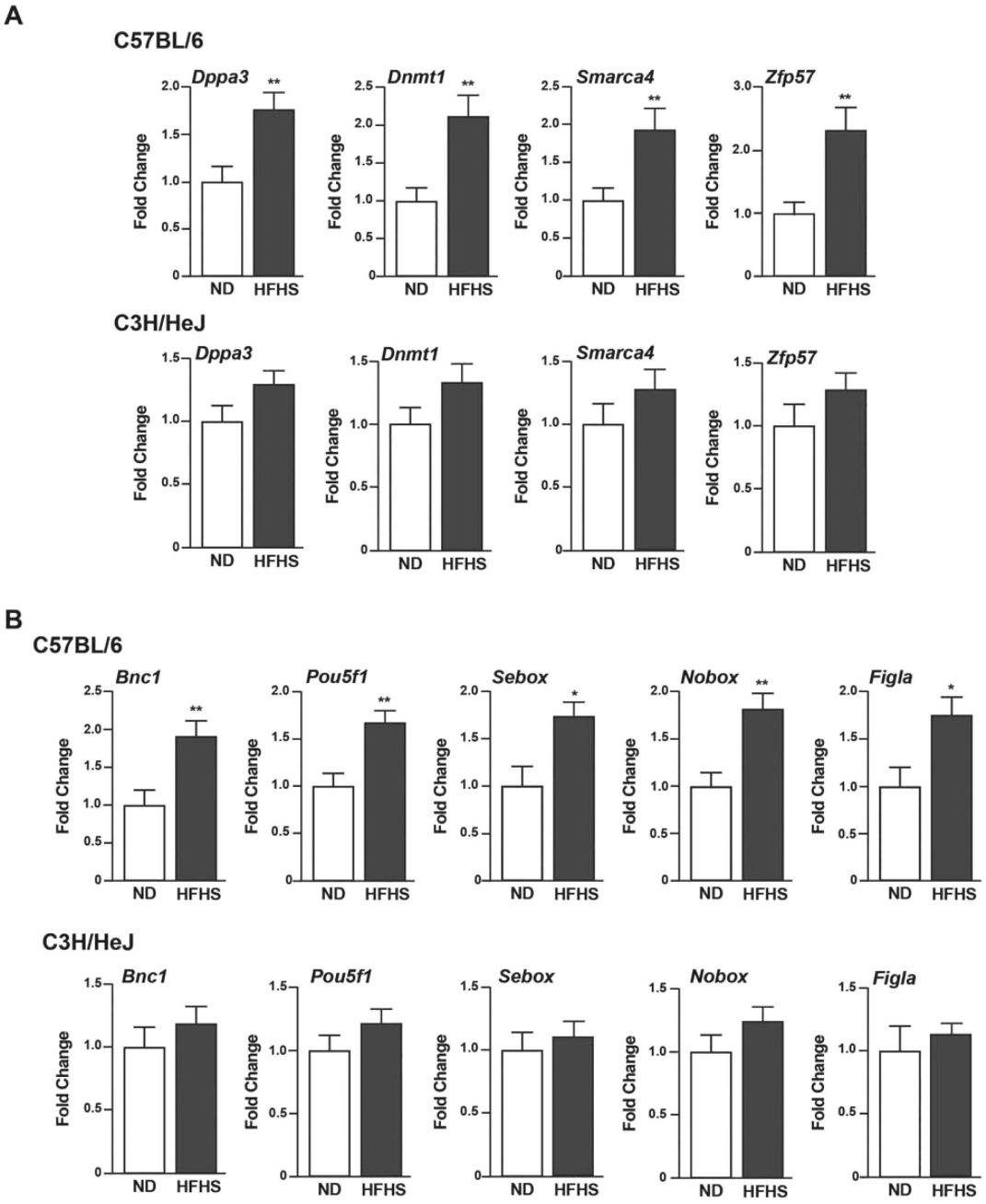

Figure 7. Oocyte gene expression of epigenetic regulators and transcription factors. Quantitative, real-time PCR analysis was performed using mRNA from oocytes from B6 and C3H mice fed control (ND; white bars) and high fat/high sugar (HFHS; black bars) diet (20 oocytes per sample; B6-ND n=11, B6-HFHS n=9, C3H-ND n=11, C3H-HFHS n=9) and primers against (A) epigenetic factors and chromatin remodeling mRNAs and (B) transcription factor mRNAs. Dppa3, developmental pluripotency associated 3; Dnmt1, DNA methyltransferase 1; Smarca4, SWI/SNF related, matrix associated, actin dependent regulator of chromatin subfamily A member 4; Zfp57, zinc finger protein 57; Bnc1, basonuclin 1; Pou5f1, POU class 5 homeobox 1; Sebox, skin- embryo- brain- and oocyte-specific homeobox protein; Nobox, newborn ovary homeobox protein; Figla, factor in germline alpha. All data are mean±SEM. **P* <0.05, ***P* <0.01, ****P* <0.001.

Discussion

Metabolic dysfunction and inflammation associated with obesity are tightly linked [13], making it difficult to delineate between the effects of hyperglycemia, excess adipose tissue, and/or inflammation on oocyte quality. In this study, we used the C57BL/6J mouse strain, which is a well-characterized model of diet-induced obesity. We also utilized C3H/HeJ mice, a sub-strain of C3H that lack a functional TLR4 and therefore are endotoxin resistant with a poor innate immune response. We confirmed that consumption of an HFHS diet induced hyperglycemia, increased percent body fat, and increased ovarian inflammation in B6 female mice. Conversely, HFHS diet consumption only induced hyperglycemia and increased percent body fat in C3H/HeJ females. Thus, inducing obesity in each mouse line using a HFHS diet allowed us to delineate the specific effects of inflammation, as opposed to hyperglycemia and/or excess adipose deposition, on oocyte quality. Indeed, others have compared C57BL/6 J and C3H/HeJ mice to identify inflammation-dependent differences in tumor development [63], atherosclerosis [64, 65], platelet aggregation response [66], and macrophage function due to endotoxin resistance [67]. We recognized that using two different inbred lines of mice could lead to the identification of genetic, rather than inflammation-dependent differences in oocyte quality; therefore, we did not make direct statistical comparisons between the two mouse lines in our study. However, Pfeiffer et al. [68] compared the transcriptome and proteome of oocytes from C57BL/6J, DBA/2J, 129/Sv, and C3H/HeN (a substrain of C3H with a functional TLR4) mice to detect genetic differences in oocyte mRNAs and proteins. While there was high variability in the expression of some genes and proteins between the mouse lines, maternal effect gene mRNA and protein levels were similar across the four groups.

One striking observation in our study was the significant decrease in embryo development to blastocyst after IVF of oocytes from B6-HFHS, but not C3H-HFHS mice. There was also decreased expression of genes (i.e., *Has2, Ptx3,* and *Tnfaip6*) in cumulus cells from both B6-HFHS and C3HHFHS mice compared to their ND counterparts. These genes encode components of the cumulus cell matrix and/or promote expansion of cumulus cells upon stimulation by the LH surge

[69]. Therefore, sufficient expression of these genes is a predictor of oocyte competence for fertilization [70]. Based on the embryo development data, the HFHS-dependent decreases in cumulus cell gene expression in both B6 and C3H mice were unexpected. Previous studies demonstrate that the expanded cumulus layer titrates the amount of glucose and fatty acids that reach the oocyte, ensuring protection against metabolic toxicity [71, 72]. Furthermore, an intact cumulus layer is an important protectant from oxidative stress associated with inflammation [73]. Thus, it may be that the hyperglycemia and increased adiposity of C3H mice affected cumulus cell gene expression, but the oocyte was protected in the absence of inflammation. Conversely, the combination of metabolic dysfunction and inflammation in B6 mice may have overcome the protective effects of cumulus cells leading to impaired oocyte quality.

Indicators of reduced oocyte developmental competence include the failure to resume meiosis and abnormal chromosomal segregation [8, 74–76]. However, there were no differences in spindle conformation or chromatin alignment in oocytes from B6-ND versus B6-HFHS or C3H-ND versus C3H-HFHS mice. This phenotypic difference between studies is likely due to differences in experimental models of obesity. To induce obesity in the current study, a diet with excess lipid and sugar was fed for only 4 weeks. Conversely, previously published studies used mice fed higher fat content for 12 to 24 weeks [8, 28, 76, 77], have induced uncontrolled hyperglycemia using streptozotocin [74–76], or have utilized mice with a genetic mutation that resulted in long-term progressive obesity [7, 27]. While meiotic maturation was not affected, the majority of maternal effect gene transcripts that were measured in each experimental group had increased abundance in oocytes from B6-HFHS compared to B6-ND mice. This outcome was consistent with previous studies using oocytes from diet-induced or genetic mouse models of obesity and oocytes from obese women with or without PCOS [13, 27–29]. Furthermore, there were no differences in the abundances of any of the candidate mRNAs in oocytes from C3H-HFHS and C3H-ND mice. Thus, these data suggest that inflammation and/or oxidative stress alters key components of mRNA metabolism resulting in either increased transcription or decreased degradation of mRNAs. The consequence of altered mRNA metabolism is an increased relative dosage of specific gene transcripts

during fertilization and prior to embryonic genome activation which may result in increased translation of proteins that interfere with essential processes during embryo development. On the other hand, the process of translation is coupled to mRNA degradation [78]; thus, the increased abundance of mRNAs may reflect reduced translational activity and therefore reduced protein levels similar to maternal effect gene knockdown models. Additional studies are required to distinguish between these two possibilities. Regardless, it is reasonable to expect that the increases in maternal effect gene mRNAs made a significant contribution to the reduced percentage of blastocysts and hatched blastocysts produced when oocytes from B6-HFHS mice were in vitro fertilized and cultured.

RBPs are important post-transcriptional regulators of mRNA translation and degradation. In the current study, zinc finger protein 36 like 2 (*Zfp36l2)* and embryonic lethal abnormal vision-like 1 (*Elavl1*) mRNAs, which encode RBPs, were increased in B6-HFHS compared to B6-ND oocytes. These proteins competitively bind to AU-rich regions within the 3′UTR of mRNAs [79, 80]. In the oocyte, ZFP36L2 binds to CNOT6L within the CCR4-NOT complex, which promotes deadenylation and represses mRNA translation [81, 82]. Mice with a truncated *Zfp36l2* transcript have decreased female fertility due, in part, to defects in resumption of meiosis and termination of development at the two-cell stage [83, 84]. In *Cnot6l* knockout mice, the degradation and clearance of maternal mRNAs during maturation and at zygotic genome activation is impaired [81]. Conversely, ELAVL1 (aka human antigen R, HuR) inhibits both RNA degradation and translation upon binding to the AU-rich 3′UTR [85]. While the effect of altered *Elavl1* expression during oocyte growth and maturation has not been determined, knockdown and overexpression of *Elavl1* during spermatogenesis results in male sterility due to impaired meiosis and disrupted translation of proteins at the spermatid stage, respectively [86]. Together, these data suggest that altered translation of ZFP36L2 and/or ELAVL1 and the relative abundance of ZFP36L2 to ELAVL1 may represent a mechanism of increased maternal transcripts in the oocytes from B6-HFHS mice.

One group of maternal effect gene mRNAs that were quantified encode SCMC proteins. The SCMC is a structural complex composed of NLRP5 (NLR family pyrin domain containing 5; aka MATER),

KHDC3 (KH domain containing protein 3, aka FILIA), OOEP (oocyte expressed protein, aka FLOPED), TLE6 (TLE family member 6), PADI6 (peptidyl arginine deiminase 6), ZBED3 (zinc finger BED-type containing 3), and NLRP2 (NLR family pyrin domain containing 2) proteins [87]. Loss of PADI6, MATER, ZBED3, or NLRP4F protein prevents normal spindle structure and chromosome alignment and the redistribution of mitochondria and endoplasmic reticulum during oocyte maturation [41,88–92]. During embryonic development, SCMC proteins persist and regulate mitotic spindle organization and symmetric division of blastomeres [93,94]. In the current study *Nlrp5 (Mater)* and *Padi6* mRNAs were increased in the B6-HFHS but not C3H-HFHS oocyte. Based on these collective data, there may be a link between altered mRNA metabolism and other key events during oocyte maturation and embryo development including mitochondrial redistribution and cell cleavage.

The expression of transcripts that encode epigenetic modulators (*Dnmt1, Smarca4,* and *Zfp57*) were also increased in B6-HFHS but not C3H-HFHS oocytes (Figure 7A). The *Smarca4* gene encodes Brahma related gene 1 (BRG1), which is an ATP-dependent chromatin remodeling factor associated with the SWI/SNF complex [95]. Conditional knockout of *Smarca4* during murine oogenesis (*Brg1Zp3-Cre*) increased termination of development at the two-cell stage and global reduction in gene transcription during zygotic genome activation [96]. In bovine oocytes, BRG-1 co-localizes with condensing chromatin during in vitro oocyte maturation [97]. Zincfinger protein 57 (ZFP57) regulates DNA methylation and its loss results in abnormal methylation of maternally imprinted genes [98,99]. DNA methyltransferase 1 (DNMT1) regulates maintenance of DNA methylation marks. In the oocyte, it specifically regulates methylation of paternally imprinted genes. As noted in the results, approximately 50% of the embryos derived from B6-HFHS oocytes were morphologically normal at the blastocyst stage. These data suggest that there may be epigenetic changes in the TE or ICM cells that could at the cellular level that could contribute to embryo loss post-implantation.

Taken together, we propose that short-term exposure to inflammation alone or the combination of inflammation and metabolic dysfunction reduces oocyte developmental competence due to abnormalities in cytoplasmic maturation. The increases in maternal effect

gene expression in this and previous studies suggest that there are abnormalities in mRNA metabolism with the end result of increased or decreased proteins that regulate key milestones in embryo development. Likewise, we hypothesize that there may be a delay in the clearance of maternal mRNAs post-fertilization which interferes with activation of the embryonic genome and the expression of embryo specific genes important for continued development.

Funding Nebraska Tobacco Settlement Biomedical Research Enhancement Funds and National Institute of Food and Agriculture Hatch Multistate Research Capacity Funding (USDA 1013511).

Supplementary material follows the References.

Data availability Data underlying this article will be shared on reasonable request to the corresponding author.

Acknowledgment The authors thank Terri Fangman and Joe Zhou from the UNL Center for Biotechnology Microscopy Core (Nebraska Research Initiative) for assistance with confocal imaging.

References

1. Hales CM, Carroll MD, Fryar CD, Ogden CL. Prevalence of obesity and severe obesity among adults: United States, 2017– 2018. *NCHS Data Brief* 2020; **360**:1–8.
2. Hanson B, Johnstone E, Dorais J, Silver B, Peterson CM, Hotaling J. Female infertility, infertility-associated diagnoses, and comorbidities: a review. *J Assist Reprod Genet* 2017; **34**:167–177.
3. Luke B, Brown MB, Stern JE, Missmer SA, Fujimoto VY, Leach R, A SART Writing Group. Female obesity adversely affects assisted reproductive technology (ART) pregnancy and live birth rates†. *Hum Reprod* 2011; **26**:245–252.
4. Luke B. Adverse effects of female obesity and interaction with race on reproductive potential. *Fertil Steril* 2017; **107**:868–877.
5. Maheshwari A, Stofberg L, Bhattacharya S. Effect of overweight and obesity on assisted reproductive technology—a systematic review. *Hum Reprod Update* 2007; **13**:433–444.
6. Dağ ZÖ, Dilbaz B. Impact of obesity on infertility in women. *J Turk Ger Gynecol Assoc* 2015; **16**:111–117.
7. Wu LL, Russell DL, Wong SL, Chen M, Tsai T-S, St John JC, Norman RJ, Febbraio MA, Carroll J, Robker RL. Mitochondrial dysfunction in oocytes of obese mothers: transmission to offspring and reversal by pharmacological endoplasmic reticulum stress inhibitors. *Development* 2015; **142**:681–691.

8. Yun Y, Wei Z, Hunter N. Maternal obesity enhances oocyte chromosome abnormalities associated with aging. *Chromosoma* 2019; **128**:413–421.
9. Chang AS, Dale AN, Moley KH. Maternal diabetes adversely affects preovulatory oocyte maturation, development, and granulosa cell apoptosis. *Endocrinology* 2005; **146**:2445–2453.
10. Rao A, Satheesh A, Nayak G, Poojary PS, Kumari S, Kalthur SG, Mutalik S, Adiga SK, Kalthur G. High-fat diet leads to elevated lipid accumulation and endoplasmic reticulum stress in oocytes, causing poor embryo development. *Reprod Fertil Dev* 2020; **32**: 1169–1179.
11. Ratchford AM, Esguerra CR, Moley KH. Decreased oocytegranulosa cell gap junction communication and connexin expression in a type 1 diabetic mouse model. *Mol Endocrinol* 2008; **22**: 2643–2654.
12. Robker RL. Evidence that obesity alters the quality of oocytes and embryos. *Pathophysiology* 2008; **15**:115–121.
13. Snider AP, Wood JR. Obesity induces ovarian inflammation and reduces oocyte quality. *Reproduction* 2019; **158**:R79–R90.
14. Spritzer PM, Lecke SB, Satler F, Morsch DM. Adipose tissue dysfunction, adipokines, and low-grade chronic inflammation in polycystic ovary syndrome. *Reproduction* 2015; **149**:R219–R227.
15. Robker RL, Wu LLY, Yang X. Inflammatory pathways linking obesity and ovarian dysfunction. *J Reprod Immunol* 2011; **88**: 142–148.
16. Akash MSH, Rehman K, Liaqat A. Tumor necrosis factor-alpha: role in development of insulin resistance and pathogenesis of type 2 diabetes mellitus. *J Cell Biochem* 2018; **119**:105–110.
17. Kawai T, Autieri MV, Scalia R. Adipose tissue inflammation and metabolic dysfunction in obesity. *Am J Physiol Cell Physiol* 2021; **320**:C375–C391.
18. Tilg H, Zmora N, Adolph TE, Elinav E. The intestinal microbiota fuelling metabolic inflammation. *Nat Rev Immunol* 2020; **20**: 40–54.
19. Rogero MM, Calder PC. Obesity, inflammation, Toll-like receptor 4 and fatty acids. *Nutrients* 2018; **10**:432.
20. Wu LL-Y, Dunning KR, Yang X, Russell DL, Lane M, Norman RJ, Robker RL. High-fat diet causes lipotoxicity responses in cumulus-oocyte complexes and decreased fertilization rates. *Endocrinology* 2010; **151**:5438–5445.
21. Desmet KLJ, Marei WFA, Richard C, Sprangers K, Beemster GTS, Meysman P, Laukens K, Declerck K, Vanden Berghe W, Bols PEJ, Hue I, Leroy JLMR. Oocyte maturation under lipotoxic conditions induces carryover transcriptomic and functional alterations during post-hatching development of good-quality blastocysts: novel insights from a bovine embryo-transfer model. *Hum Reprod* 2020; **35**:293–307.
22. Sohrabi M, Mohammadi Roushandeh A, Alizadeh Z, Vahidinia A, Vahabian M, Hosseini M. Effect of a high fat diet on ovary morphology, in vitro development, in vitro fertilisation rate and oocyte quality in mice. *Singapore Med J* 2015; **56**:573–579.
23. Grindler NM, Moley KH. Maternal obesity, infertility, and mitochondrial dysfunction: potential mechanisms emerging from mouse model systems. *Mol Hum Reprod* 2013; **19**: 486–494.

24. Bromfield JJ, Sheldon IM. Lipopolysaccharide initiates inflammation in bovine granulosa cells via the TLR4 pathway and perturbs oocyte meiotic progression in vitro. *Endocrinology* 2011; **152**: 5029–5040.
25. Zhao S, Pang Y, Zhao X, Du W, Hao H, Zhu H. Detrimental effects of lipopolysaccharides on maturation of bovine oocytes. *Asian-Australas J Anim Sci* 2019; **32**:1112–1121.
26. Piersanti RL, Santos JEP, Sheldon IM, Bromfield JJ. Lipopolysaccharide and tumor necrosis factor-alpha alter gene expression of oocytes and cumulus cells during bovine in vitro maturation. *Mol Reprod Dev* 2019; **86**:1909–1920.
27. Pohlmeier WE, Xie F, Kurz SG, Lu N, Wood JR. Progressive obesity alters the steroidogenic response to ovulatory stimulation and increases the abundance of mRNAs stored in the ovulated oocyte. *Mol Reprod Dev* 2014; **81**:735–747.
28. Xie F, Anderson CL, Timme KR, Kurz SG, Fernando SC, Wood JR. Obesity-dependent increases in oocyte mRNAs are associated with increases in proinflammatory signaling and gut microbial abundance of Lachnospiraceae in female mice. *Endocrinology* 2016; **157**:1630–1643.
29. Wood JR, Dumesic DA, Abbott DH, Strauss JF 3rd. Molecular abnormalities in oocytes from women with polycystic ovary syndrome revealed by microarray analysis. *J Clin Endocrinol Metab* 2007; **92**:705–713.
30. Wu X, Brewer G. The regulation of mRNA stability in mammalian cells: 2.0. *Gene* 2012; **500**:10–21.
31. Gosden RG. Oogenesis as a foundation for embryogenesis. *Mol Cell Endocrinol* 2002; **186**:149–153.
32. Brower PT, Gizang E, Boreen SM, Schultz RM. Biochemical studies of mammalian oogenesis: synthesis and stability of various classes of RNA during growth of the mouse oocyte in vitro. *Dev Biol* 1981; **86**:373–383.
33. Medvedev S, Pan H, Schultz RM. Absence of MSY2 in mouse oocytes perturbs oocyte growth and maturation, RNA stability, and the transcriptome. *Biol Reprod* 2011; **85**:575–583.
34. Christou-Kent M, Dhellemmes M, Lambert E, Ray PF, Arnoult C. Diversity of RNA-binding proteins modulating posttranscriptional regulation of protein expression in the maturing mammalian oocyte. *Cell* 2020; **9**:662–662.
35. Svoboda P, Franke V, Schultz RM. Sculpting the transcriptome during the oocyte-to-embryo transition in mouse. *Curr Top Dev Biol* 2015; **113**:305–339.
36. Condic ML. The role of maternal-effect genes in mammalian development: are mammalian embryos really an exception? *Stem Cell Rev Rep* 2015; **12**:276–284.
37. Zuccotti M, Merico V, Sacchi L, Bellone M, Brink TC, Bellazzi R, Stefanelli M, Redi CA, Garagna S, Adjaye J. Maternal Oct-4 is a potential key regulator of the developmental competence of mouse oocytes. *BMC Dev Biol* 2008; **8**:97–97.
38. Tripurani SK, Lee KB, Wang L, Wee G, Smith GW, Lee YS, Latham KE, Yao J. A novel functional role for the oocyte-specific transcription factor newborn ovary homeobox (NOBOX) during early embryonic development in cattle. *Endocrinology* 2011; **152**: 1013–1023.
39. Payer B, Saitou M, Barton SC, Thresher R, Dixon JPC, Zahn D, Colledge WH, Carlton MBL, Nakano T, Surani MA. Stella is a maternal effect gene required for normal early development in mice. *Curr Biol* 2003; **13**:2110–2117.

40. Mtango NR, Sutovsky M, Susor A, Zhong Z, Latham KE, Sutovsky P. Essential role of maternal UCHL1 and UCHL3 in fertilization and preimplantation embryo development. *J Cell Physiol* 2012; **227**:1592–1603.
41. Tashiro F, Kanai-Azuma M, Miyazaki S, Kato M, Tanaka T, Toyoda S, Yamato E, Kawakami H, Miyazaki T, Miyazaki J-I. Maternal-effect gene Ces5/Ooep/Moep19/Floped is essential for oocyte cytoplasmic lattice formation and embryonic development at the maternal-zygotic stage transition. *Genes Cells* 2010; **15**: 813–828.
42. Avilion AA, Nicolis SK, Pevny LH, Perez L, Vivian N, Lovell-Badge R. Multipotent cell lineages in early mouse development depend on SOX2 function. *Genes Dev* 2003; **17**:126–140.
43. Poltorak A, He X, Smirnova I, Liu MY, Van Huffel C, Du X, Birdwell D, Alejos E, Silva M, Galanos C, Freudenberg M, Ricciardi-Castagnoli P *et al.* Defective LPS signaling in C3H/HeJ and C57BL/10ScCr mice: mutations in Tlr4 gene. *Science* 1998; **282**:2085–2088.
44. Lu Y-C, Yeh W-C, Ohashi PS. LPS/TLR4 signal transduction pathway. *Cytokine* 2008; **42**:145–151.
45. Rosario FJ, Kanai Y, Powell TL, Jansson T. Increased placental nutrient transport in a novel mouse model of maternal obesity with fetal overgrowth. *Obesity (Silver Spring)* 2015; **23**:1663–1670.
46. Pasquariello R, Ermisch AF, Silva E, Mccormick S, Logsdon D, Barfield JP, Schoolcraft WB, Krisher RL. Alterations in oocyte mitochondrial number and function are related to spindle defects and occur with maternal aging in mice and humans †. *Biol Reprod* 2018; **100**:971–981.
47. Choi W-J, Banerjee J, Falcone T, Bena J, Agarwal A, Sharma RK. Oxidative stress and tumor necrosis factor–*α*–induced alterations in metaphase II mouse oocyte spindle structure. *Fertil Steril* 2007; **88**:1220–1231.
48. Herrick JR, Krisher RL, Strauss KJ, Schneiderman BA, Rawlins M, Stevens J, Schoolcraft WB. The beneficial effects of reduced magnesium during the oocyte-to-embryo transition are conserved in mice, domestic cats, and humans. *Reprod Fertil Dev* 2013; **27**:323–331.
49. Silva E, Greene AF, Strauss K, Herrick JR, Schoolcraft WB, Krisher RL. *Antioxidant supplementation during in vitro culture improves mitochondrial function and development of embryos from aged female mice*. *Reprod Fertil Dev* 2015; **27**:975–983.
50. Bakhtari A, Ross PJ. DPPA3 prevents cytosine hydroxymethylation of the maternal pronucleus and is required for normal development in bovine embryos. *Epigenetics* 2014; **9**:1271–1279.
51. Ermisch AF, Herrick JR, Pasquariello R, Dyer MC, Lyons SM, Broeckling CD, Rajput SK, Schoolcraft WB, Krisher RL. A novel culture medium with reduced nutrient concentrations supports the development and viability of mouse embryos. *Sci Rep* 2020; **10**:9263.
52. Mack EM, Smith JE, Kurz SG, Wood JR. CAMP-dependent regulation of ovulatory response genes is amplified by IGF1 due to synergistic effects on Akt phosphorylation and NF-kB transcription factors. *Reproduction* 2012; **144**:595–602.

53. Mamo S, Gal AB, Bodo S, Dinnyes A. Quantitative evaluation, and selection of reference genes in mouse oocytes and embryos cultured in vivo and in vitro. *BMC Dev Biol* 2007; **7**:1–12.
54. Filatov MA, Nikishin DA, Khramova YV, Semenova ML, Koltzov NK. Reference genes selection for real-time quantitative PCR analysis in mouse germinal vesicle oocytes. *Zygote* 2019; **27**:392–397.
55. Mack EM, Smith JE, Kurz SG, Wood JR. cAMP-dependent regulation of ovulatory response genes is amplified by IGF1 due to synergistic effects on Akt phosphorylation and NF-κB transcription factors. *Reproduction* 2012; **144**:595–602.
56. Chistiakov DA, Killingsworth MC, Myasoedova VA, Orekhov AN, Bobryshev YV. CD68/macrosialin: not just a histochemical marker. *Lab Invest* 2017; **97**:4–13.
57. Morris G, Gevezova M, Sarafian V, Maes M. Redox regulation of the immune response. *Cell Mol Immunol* 2022; **19**:1079–1101.
58. Arango Duque G, Descoteaux A. Macrophage cytokines: involvement in immunity and infectious diseases. *Front Immunol* 2014; **5**:491.
59. He L, He T, Farrar S, Ji L, Liu T, Ma X. Antioxidants maintain cellular redox homeostasis by elimination of reactive oxygen species. *Cell Physiol Biochem* 2017; **44**:532–553.
60. Jarukamjorn K, Jearapong N, Pimson C, Chatuphonprasert W. A high-fat, high-fructose diet induces antioxidant imbalance and increases the risk and progression of nonalcoholic fatty liver disease in mice. *Scientifica (Cairo)* 2016; **2016**:5029414.
61. Dali-Youcef N, Lagouge M, Froelich S, Koehl C, Schoonjans K, Auwerx J. Sirtuins: the 'magnificent seven', function, metabolism, and longevity. *Ann Med* 2007; **39**:335–345.
62. Uyar A, Torrealday S, Seli E. Cumulus and granulosa cell markers of oocyte and embryo quality. *Fertil Steril* 2013; **99**:979–997.
63. Bursch W, Grasl-Kraupp B, Wastl U, Hufnagl K, Chabicovsky M, Taper H, Schulte-Hermann R. Role of apoptosis for mouse liver growth regulation and tumor promotion: comparative analysis of mice with high (C3H/He) and low (C57Bl/6J) cancer susceptibility. *Toxicol Lett* 2004; **149**:25–35.
64. Shi W, Wang NJ, Shih DM, Sun VZ, Wang X, Lusis AJ. Determinants of atherosclerosis susceptibility in the C3H and C57BL/6 mouse model: evidence for involvement of endothelial cells but not blood cells or cholesterol metabolism. *Circ Res* 2000; **86**: 1078–1084.
65. Potier M, Karl M, Elliot SJ, Striker GE, Striker LJ. Response to sex hormones differs in atherosclerosis-susceptible and -resistant mice. *Am J Physiol Endocrinol Metab* 2003; **285**:E1237–E1245.
66. Paigen B, Kovats SE, Chapman MH, Lin CY. Characterization of a genetic difference in the platelet aggregation response of two inbred mouse strains, C57BL/6, and C3H/He. *Atherosclerosis* 1987; **64**: 181–190.
67. Shou J, Redmond HP, Leon P, Hofmann KP, Daly JM. Elemental diet alters macrophage function in mice. *J Surg Res* 1991; **51**: 192–196.
68. Pfeiffer MJ, Taher L, Drexler H, Suzuki Y, Makałowski W, Schwarzer C, Wang B, Fuellen G, Boiani M. Differences in embryo quality are associated with

differences in oocyte composition: a proteomic study in inbred mice. *Proteomics* 2015; **15**:675–687.
69. Russell DL, Salustri A. Extracellular matrix of the cumulus-oocyte complex. *Semin Reprod Med* 2006; **24**:217–227.
70. Patil K, Shinde G, Hinduja I, Mukherjee S. Compromised cumulusoocyte complex matrix organization and expansion in women with PCOS. *Reprod Sci* 2022; **29**:836–848.
71. Lolicato F, Brouwers JF, de Lest CH, Wubbolts R, Aardema H, Priore P, Roelen BAJ, Helms JB, Gadella BM. The cumulus cell layer protects the bovine maturing oocyte against fatty acid-induced lipotoxicity. *Biol Reprod* 2015; **92**:16.
72. Dunning KR, Watson LN, Sharkey DJ, Brown HM, Norman RJ, Thompson JG, Robker RL, Russell DL. Molecular filtration properties of the mouse expanded cumulus matrix: controlled supply of metabolites and extracellular signals to cumulus cells and the oocyte. *Biol Reprod* 2012; **87**:89.
73. Shaeib F, Khan SN, Ali I, Thakur M, Saed MG, Dai J, Awonuga AO, Banerjee J, Abu-Soud HM. The defensive role of cumulus cells against reactive oxygen species insult in metaphase II mouse oocytes. *Reprod Sci* 2016; **23**:498–507.
74. Colton SA, Pieper GM, Downs SM. Altered meiotic regulation in oocytes from diabetic mice. *Biol Reprod* 2002; **67**:220–231.
75. Colton SA, Humpherson PG, Leese HJ, Downs SM. Physiological changes in oocyte-cumulus cell complexes from diabetic mice that potentially influence meiotic regulation. *Biol Reprod* 2003; **69**: 761–770.
76. Wang Q, Ratchford AM, Chi MM-Y, Schoeller E, Frolova A, Schedl T, Moley KH. Maternal diabetes causes mitochondrial dysfunction and meiotic defects in murine oocytes. *Mol Endocrinol* 2009; **23**:1603–1612.
77. Jungheim ES, Schoeller EL, Marquard KL, Louden ED, Schaffer JE, Moley KH. Diet-induced obesity model: abnormal oocytes and persistent growth abnormalities in the offspring. *Endocrinology* 2010; **151**:4039–4046.
78. Roy B, Jacobson A. The intimate relationships of mRNA decay and translation. *Trends Genet* 2013; **29**:691–699.
79. Wang H, Ding N, Guo J, Xia J, Ruan Y. Dysregulation of TTP and HuR plays an important role in cancers. *Tumor Biol* 2016; **37**:14451–14461.
80. Uchida Y, Chiba T, Kurimoto R, Asahara H. Post-transcriptional regulation of inflammation by RNA-binding proteins via ciselements of mRNAs. *J Biochem* 2019; **166**:375–382.
81. Sha Q-Q, Yu J-L, Guo J-X, Dai X-X, Jiang J-C, Zhang Y-L, Yu C, Ji S-Y, Jiang Y, Zhang S-Y, Shen L, Ou X-H *et al.* CNOT6L couples the selective degradation of maternal transcripts to meiotic cell cycle progression in mouse oocyte. *EMBO J* 2018; **37**:e99333.
82. Gillen SL, Giacomelli C, Hodge K, Zanivan S, Bushell M, Wilczynska A. Differential regulation of mRNA fate by the human Ccr4-Not complex is driven by coding sequence composition and mRNA localization. *Genome Biol* 2021; **22**:284.
83. Ball CB, Rodriguez KF, Stumpo DJ, Ribeiro-Neto F, Korach KS, Blackshear PJ, Birnbaumer L, Ramos SBV. The RNA-binding protein, ZFP36L2, influences ovulation and oocyte maturation. *PLoS One* 2014; **9**:e97324.

84. Ramos SBV, Stumpo DJ, Kennington EA, Phillips RS, Bock CB, Ribeiro-Neto F, Blackshear PJ. The CCCH tandem zinc-finger protein Zfp36l2 is crucial for female fertility and early embryonic development. *Development* 2004; **131**:4883–4893.
85. Liu R, Wu K, Li Y, Sun R, Li X. Human antigen R: a potential therapeutic target for liver diseases. *Pharmacol Res* 2020; **155**:104684.
86. Chi MN, Auriol J, Jégou B, Kontoyiannis DL, Turner JMA, de Rooij DG, Morello D. The RNA-binding protein ELAVL1/HuR is essential for mouse spermatogenesis, acting both at meiotic and postmeiotic stages. *MBoC* 2011; **22**:2875–2885.
87. Lu X, Gao Z, Qin D, Li L. A maternal functional module in the mammalian oocyte-to-embryo transition. *Trends Mol Med* 2017; **23**:1014–1023.
88. Kim B, Zhang X, Kan R, Cohen R, Mukai C, Travis AJ, Coonrod SA. The role of MATER in endoplasmic reticulum distribution and calcium homeostasis in mouse oocytes. *Dev Biol* 2014; **386**: 331–339.
89. Gao Z, Zhang X, Yu X, Qin D, Xiao Y, Yu Y, Xiang Y, Nie X, Lu X, Liu W, Yi Z, Li L. Zbed3 participates in the subcortical maternal complex and regulates the distribution of organelles. *J Mol Cell Biol* 2018; **10**:74–88.
90. Qin D, Gao Z, Xiao Y, Zhang X, Ma H, Yu X, Nie X, Fan N, Wang X, Ouyang Y, Sun Q-Y, Yi Z *et al.* The subcortical maternal complex protein Nlrp4f is involved in cytoplasmic lattice formation and organelle distribution. *Development* 2019; **146**:dev183616.
91. Kim B, Kan R, Anguish L, Nelson LM, Coonrod SA. Potential role for MATER in cytoplasmic lattice formation in murine oocytes. *PLoS One* 2010; **5**:e12587.
92. Kan R, Yurttas P, Kim B, Jin M, Wo L, Lee B, Gosden R, Coonrod SA. Regulation of mouse oocyte microtubule and organelle dynamics by PADI6 and the cytoplasmic lattices. *Dev Biol* 2011; **350**: 311–322.
93. Yu X-J, Yi Z, Gao Z, Qin D, Zhai Y, Chen X, Ou-Yang Y, Wang Z-B, Zheng P, Zhu M-S, Wang H, Sun Q-Y *et al.* The subcortical maternal complex controls symmetric division of mouse zygotes by regulating F-actin dynamics. *Nat Commun* 2014; **5**: 4887.
94. Zheng P, Dean J. Role of Filia, a maternal effect gene, in maintaining euploidy during cleavage-stage mouse embryogenesis. *PNAS* 2009; **106**:7473–7478.
95. Ho L, Crabtree GR. Chromatin remodelling during development. *Nature* 2010; **463**:474–484.
96. Bultman SJ, Gebuhr TC, Pan H, Svoboda P, Schultz RM, Magnuson T. Maternal BRG1 regulates zygotic genome activation in the mouse. *Genes Dev* 2006; **20**:1744–1754.
97. Wee G, Shin S-T, Koo D-B, Han Y-M. Behaviors of ATP-dependent chromatin remodeling factors during maturation of bovine oocytes in vitro. *Mol Reprod Dev* 2010; **77**:126–135.
98. Li X, Ito M, Zhou F, Youngson N, Zuo X, Leder P, Ferguson- Smith AC. A maternal-zygotic effect gene, Zfp57, maintains both maternal and paternal imprints. *Dev Cell* 2008; **15**:547–557.
99. Hanna CW, Kelsey G. The specification of imprints in mammals. *Heredity (Edinb)* 2014; **113**:176–183.

Supplementary Table 1. Primers used for qPCR of oocytes and cumulus cells

Gene	Accession No.	Forward Primer (5'→3')	Reverse Primer (5'→3')	Location
Oocytes				
Bnc1	NM_007562.2	TGCAGGATGGCTGAGGCTATCG	ACTGTTCACACTGACGGTGGTT	91-181
Dnmt1	NM_001199431.1	ACATGCAGCTTTCCTACATCCA	ATGGAGGGAGGCACAGACC	2557-2643
Dppa3	NM_139218.1	GTTCGGATTGAGCAGAGACAAA	TGAACGGGACAGTGAGCCA	415-477
Elavl1	NM_010485	ACACAGCTTGGGCTACGGTT	TGGGCGAGCATATGACACCTTA	405-525
Figla	NM_012013.2	GCGTGAACGGATAAAAAATCTCA	CTGAAGGCTCTGGTGCCG	258-315
Gdf9	NM_008110.2	GCCGGGCAAGTACAGCC	TTTGTAAGCGATGGAGCCG	1249-1312
Gpx	NM_008160	CGAGATGAACGATCTGCAGAAG	ATTCTCCTGGTGTCCGAACTGA	398-485
Khdc3	NM_025890.3	CCCTGAAAGGCGAGCTGAGA	AGCCTCCAGAGCCTCTATTTCC	349-475
Nlrp5	NM_011860.3	CCTGCGAAGCGCTGAAA	ACTCTGAGGTTGGATTCCTGTGA	2322-2382
Nobox	NM_130869.3	TGGGGCACTAGTATCGCCT	GGGTAAATGTGGAGCCTGGGA	986-1105
Ooep	NM_026480.3	AAAACGAACTCCAAAGAGCTGTGA	AAAGCCAGCCAGTTTTAGCCC	401-513
Padi6	NM_153106.2	CCGTCATCGCTGGCAAAGAG	AGTAGGAGACCAGCACCTTGT	227-349
Pou5f1	NM_013633.3	GAGGAGTCCCAGGACATGAAAG	GTTTGCCAAGCTGCTGAAGC	440-503
Sebox	NM_008759.3	CTTTCAGTGTCGGGCAGTTGG	GATTCTGGAACCACACCTGGAT	119-253
Sirt1	NM_019812	GCCGCGGATAGGTCCATATA	TCGAGGATCGGTGCCAAT	575-635
Sod1	NM_011434	GTGCAGGGAACCATCCACTT	GTCCTGACAACACAACTGGTTCA	159-219
Smarca4	NM_001174078.1	TCAGCTCAGCGAGGTGTTCA	GGTTTCGGATGCGTTCCTTGA	4607-4719
Tle6	NM_053254.2	GATCCCTGGGGCCTCCCTAAC	CGACTGGATAAGGTGGAAGGCAAAA	73-204
Uchl1	NM_011670.2	AGGGCCAGTGTCGGGTAGAT	CACTGGAAAGGGCATTCGCC	615-718
Zar1	NM_174877.3	ACTAGATGTGCCTGCCCAGT	TGAGCTTTCTCCCCTCTTCA	982-1182
Zfp57	NM_001001806.2	TGTGGCTAGAAGCAGTCTGGAA	TGGATGGCTGGGAAGACTGTT	310-406
H2az1	NM_016750.3	GTATAAAGGGCGCGAGGAAGG	TACCGCCAGCCATCTCGG	71-220
Cumulus Cells				
Has2	NM_008216	ACAGGCGGAGGACGAGTCTA	TGATTCCGAGGAGGAGAGACA	515-632
Ptgs2	NM_011198	TGGGCCATGGAGTGGACTT	GGGATACACCTCTCCACCAATG	729-847
Ptx3	NM_008987	GGACAACGAAATAGACAATGGACTT	CGAGTTCTCCAGCATGATGAAC	265-373
Tnfaip6	NM_009398	GATGGGATGCCTATTGCTACAAC	TCGCTTCGGATCTGTGAAGA	428-295
Actb	NM_007393	AGATGACCCAGATCATGTTTGAGA	CACAGCCTGGATGGCTACGT	432-496

Supplementary Table 2. gBlocks used for qPCR of oocytes and cumulus cells

gBlock	Sequence
Elavl1 Khdc3 Nobox Ooep	TTTGAACTGGCAGCGAAAGAACATGCAGCTTACAGCTGGATCTAAGCTGAGAGAAATGGAGTCAAACTGGGTGTC GCTGGTGAGTACCATTTCTGCTGCCACAAGGTGAAGATGTGGAAAAGATTTTGGATGAATGGAAGGAATATAAAA TGGGAGTCCCGACTTACGGTGCAATTATTCTCGATGAGACACTGGAGAATGTACTGCTGGTTCAGGGGTACCTGCA GGACACAGCTTGGGCTACGGTTTTGTGAACTATGTGACTGCAAAAGATGCAGAGAGAGCAATCAGCACACTGAAC GGCTTGAGACTCCAGTCCAAAACCATTAAGGTGTCATATGCTCGCCCAAGCTCACCGGCAGCGGCCGAACAATGA AGCTCTTGAAGCCAACCTGGGTCAACCACAATGGGAAGCCAATTTTTTCAGTTGATATTCACCCTGATGGGACCAA GTTTGCAACTGGAGGACAAGGGCAGGATTCTGGGAAGGTTGTGGGGCCCTGAAAGGCGAGCTGAGATTTGGATAT TCGGACCGCCGCCTTTCCGAAGGGACGTTGACCGGATGCTCACTGATCTGGCTCACTATTGCCGCATGAAACTGAT GGAAATAGAGGCTCTGGAGGCTGGAGTTCCTCACACACTATAAACGGCCCCATACCTTGAACAGCACCAGCATGT CTAAGGCGTATCAGAGCACCTTCACAGGCGAGACCAACACCCCGTACAGCAAGCAGTTGTCCTGGGGCACTAGTA TCGCCTCACCACCCACCTACTCAAATTTGGAAGACCTGGGGTCTCAGGACTACCAAGCAAGCAGCCAGTTGGGTTC ATTCCAGCTCTCCCAGGCTCCACATTTACCCCTTTTCAAAGAAAACGAACTCCAAAGAGCTGTGAAGGTGAAAGA AGTTGAAGAGTTCTTGAAAATTCGTGCCTCCTCAATCCTAAGCAAGTTAAGTAAGAAAGGGCTAAAACTGGCTGG CTTTCCGCT
Bnc1 Zar1	GCGGCTGCAGGATGGCTGAGGCTATCGGCTGTACTCTGAACTGCAGTTGCCAATGTTTCAAACCTGGGAAGATAA ACCACCGTCAGTGTGAACAGTGCAGGCGGACCTGACACCAGTCCCAAGGCATCAGACTTGGGGTCAGTAACTGAC TCTGATGTTGACTGTACCGATAACACACAAACCCAAAGGAAGAAGAAAAGGAAAGGGAAAGCAAGAGTGCTTAG CAAAGAATCTGTTCGTAAAGACAGAGAAAGAGGAAATGCAGGCGGGTAAGCACCAAGAATATGAACAGAAGCTC CTCCAAGAATTATATAAATTAAATCCCAATTTTCTTCAGCTATCTACGGGTTCAGTTGATAAGAATAAGAACAAAG TGACACCATTACAAAGCCCCATTGACAAACCTTCAGATACACCATCATGTCCGCAGAGGAGGTAGCCAATGGGAA AAAATCTCACTGGGCAGAGTTAGAGATCTCGGGTAGAGTGCGGAGCTTAAGTACACTATGCCAGCAGCAACCGTA GATCATAGCCAAAGAATTTGTGAAGTTTGGGCTTGTAACCTGGATGAAGAGATGAAGAAAATCCGTCAAGTTATC CGAAAATATAATTATGTTGCTATGGACACCGAGTTTCCAGGCGATGAGAGGAATCAGATGGGCGGCTCAAATATC TCCAGTCCTGGGCTACAGCCAAGCACTCAGCTCTCTAATCTGGGAAGCACCGAGACTCTAGAAGAGACACCCTCT GGGTCACAGGATAAGTCTGCTCCGTCTGGTCATAAACAAAGAACTAGATGTGCCTGCCCAGTCAGACTTCGCCAC GTGGACCCTAAACGCCCCCATCGGCAAGACTTGTGTGGGAGATGCAAGGACAAACGCCTGTCCTGCGACAGCACC TTCAGCTTCAAATACATCATTTAGTGAGAGTCGAAAACGTTTCTGCTAGATGGGGCTAATGGAATGGACAAGTGA GCTTTCTCCCCTCTTCACCTCT
Dmnt1 Dppa3 Figla Nlrp5 Pou5f1	CGAAAACATGCAGCTTTCCTACATCCACAGCAAGGTCAAGGTCATCTACAAAGCCCCTTCTGAAAACTGGGCCAT GGAGGGAGGCACAGACCCTGAGGACTTGTTCGGATTGAGCAGAGACAAAAAAGGCTCGAAGGAAATGAGTTTGA ACGGGACAGTGAGCCATTCAGCACCGAGGCCTCCATGATGATGTCCCTCACGAAGCTGGCTGACAAGGAACTGGT GCACATGATTGGCTGGGCCAAGAAAGAGCGTGAACGGATAAAAAATCTCAACCGTGGCTTTGCCAAGCTGAAGGC TCTGGTGCCGTTTCTGGTCCAGTTCAGCTCCATTTGATCAAGATCAGCTTTACACCTGGGCTGCGGTTAGTCAACCC ACACATTCGATGGATTACAGCGAAGGGCAGTTTCGCAGGCGAGAGAGGCCCTGGAAACATGGGCGACTGGGGCTT CCTGGAGAAGTTGCTAGACCAGGTCCAGGAACACTCGACCGTGGTGGGCAAGATCCCCCTCCCCACTTTCCCATAA TTCATGACATCAAAACATCGGCTTTTCCCTTGAGACTCAGGAGGGCCAAAGCACCAGCCTTTGGCTTTTTTCTCTTT TTTTTCCCTCTCCCCTAGCATGGGTTGAAGGAAGGGATCCATCCTTATTGTTCCGAGGCATCACCTCCCTCCCTAGT CAGGCTGAGAAGGAACCAGCCAGCTCATACCTCCAGTGCAAGCGGTGGCAGAAAAACCAGTGGTTGAAGACTAG CAATGGTCTGATTCAGAAGGGCTCAGCACCAGTGGTTAGCCTGCGAAGCGCTGAAACATCCAAAGTGCTCCGTGG AGACTCTGAGGTTGGATTCCTGTGAGTTAACTCCCGAGGAGTCCCAGGACATGAAAGCCCTGCAGAAGGAGCTAG AACAGTTTGCCAAGCTGCTGAAGCAGAAG
Padi6 Sebox Smarca4	TAGCTCCGTCATCGCTGGCAAAGAGGACACTGTGGTCTGGAGGTCAATGAACCATCCCACAGTGGCATTGGTGAG GATGGTGGCGCCCAGCCCCACTGTGGATGAAGACAAGGTGCTGGTCTCCTACTTCTGTTCACACTCTCCTACCCTG AGGATAAAACCGGGAAGAACTATGACTTTGCTCAGGTGCTGAAGCGAAGTATCTGCCTGGAGCAGAACACACAGG CCTGGTGTGACAACTGTGAGAAGTACCAGCCCACAATTCAGACCAGAAACGTTCCGGGCCAGGTGGACTTCTATG CGCGCTTCTCGCCGTCGCCACTCTCCATGAAGCAGTTCCTGGACTTCGGGTCAGTGAATGCTTGTGAGAAACACCG TGTAAGTGAAGAGCTGAGTGAAGAAGACTAAAATCCAGTTTATTGGATTTCAATACTATGTCCTAAAAGACAGAT AATTTTCCACTTGATCACCAAGATGGAGAACTCAGATTCTAACGATAAAGGAAGTGACCAGTCTGCAGCTCAGAC CACTTTCAGTGTCGGGCAGTTGGTGGAGCTGGAGCGGGTATTTGCAGCTAGGCCCTATCCTGACATCAGCACCCGT GAGCACCTGGCTCAGGTAACTCACCTGCCTGAAGCCAAGATCCAGGTGTGGTTCCAGAATCGGCGAGGACGTCAG CTCAGCGAGGTGTTCATCCAGCTCCCCTCTCGCAAGGAGCTTCCTGAGTACTATGAGCTCATCCGAAAGCCTGTGG ACTTCAAGAAGATCAAGGAACGCATCCGAAACCACAAGTCTAAGATGTTCCATCCTAACGTCTATGCAGATGGTA GTATATGTCTGGATATACTTCAGAACCGTTGGAGTCCAACCTATGATGTGTCTTCCATTTTAACGTCCATACAGTCT CTATTGGATGAACCTAATCCCAATAGTCCAGCAAACAGCCAGGCTG

Supplementary Table 2. gBlocks used for qPCR of oocytes and cumulus cells (continued)

Tle6 Uchl1 Zfp57 H2az1	CCAACTCTCCCGCGGTGACTGTGACTGGAGGAGTCCTGCATCCATGGAGCAAACCGAAGGCGTGAGTACAGAATG TGCTAAGGCCTCTGGGATCCCTGGGGCCTCCCTAACCTCAGAGGTGGACTTAATCAGATTTGTGACCTCAAGAATC TTCTAGATGACTTCCCACAGACAGAGCAGTGACACCTTTGGTGGAATTTTGCCTTCCACCTTATCCAGTCGGTATTC CAGGAGGGCCAGTGTCGGGTAGATGACAAAGTGAATTTCCATTTTATTCTGTTCAACAACGTGGACGGCCATCTGT ACGAGCTCGATGGGCGAATGCCCTTTCCAGTGAACCAGGCACCTCCCAACCTCCACGCTTGCAATTTCGACCATTA CAGGACCCAGAAAAATGTCGACCACACTTCTGTCACCCTTCTACGATATCGACTTCTTGTGCAAGACGGAGAAATC CCTGGCAACAAATTGTGGCTAGAAGCAGTCTGGAATAGAAGTCAAACGCCTAGGACCAGCCTGGCATTACCAAAC AATGGCAGCTAGGAAACAGTCTTCCCAGCCATCCAGGACACTGCAGTATAAAGGGCGCGAGGAAGGCGGGAGAC GGCGCAGTTTGAATCGCGGTCCGACGGAGGAGTGGGCGCTGGGATCTCGCTGAGCGTCCGCCTGGCCTCGTCTCTT CCTCGCTCGTCGGAGCTTCAGCACGGTCCGAGATGGCTGGCGGTAAGGCT
Gpx Sirt1 Sod1	CGACGGTCCGGTGCAGGGAACCATCCACTTCGAGCAGAAGGCAAGCGGTGAACCAGTTGTGTTGTCAGGACAAAT TACAGGATTAACTGAAGTACCACGAGGCTCTGGCCAAGGGAGATGTTACAACTCAGGTCGCTCTTCAGCCTGCACT GAAGTTCAATGGTGGGGGACATATTAATCACACCATTTTCTGGACAGGACTCCGCGGCCGCGGATAGGTCCATAT ACTTTTGTTCAGCAACATCTCATGATTGGCACCGATCCTCGAACAATTCTTACGGGACTACACCGAGATGAACGAT CTGCAGAAGCGTCTGGGACCTCGTGGACTGGTGGTGCTCGGTTTCCCGTGCAATCAGTTCGGACACCAGGAGAAT GGCAAGAATG
Gdf9	TGTGTGCCGGGCAAGTACAGCCCCCTGAGTGTGTTGACCATTGAACCCGACGGCTCCATCGCTTACAAAGAGTA
Ptx3 Tnfaip6 Has2 Ptgs2	ATTTGGACAACGAAATAGACAATGGACTTCATCCCACCGAGGACCCCACGCCATGCGACTGCCGCCAGGAGCACT CGGAGTGGGACAAGCTGTTCATCATGCTGGAGAACTCGCAGAGAGCGATGGGATGCCTATTGCTACAACCCACAT GCAAAGGAGTGTGGTGGTGTCTTCACAGATCCGAAGCGAATTTAGGAATTTCCCCTGACCCAGGAAGATGCCCTG CTGGCTGTGAGGAAATACTTCCACAGGATCACTGTGTACCTGAGAGAGAAGAAACACAGCCCCTGTGCCTGGGAG GTGGTCAGAGCAGAAGTCTGGAGAGCCCTGTCTTCCTCTGCCAATGTGCTGGGAAGACTAAGTACAACAGCTACG CCTGGATGGTGGTCCGAGCAGAGATCTTCAGGAACTTTCTCATCATTCGAAGACTTACCAGAAACTTCCAAAACTG AAGACCTGTCAGTTGATGCCTCAGAATGAGTGGTGGTTGCAGGCAACCTCACAGACAGGCGGAGGACGAGTCTAT GAGCAGGAGCTGAACAAGATGCATTGTGAGAGGTTTCTATGTGTCCTGAGAATAATTGGAACTACACTTTTTGGAG TGTCTCTCCTCCTCGGAATCACAGCTAGGACTGGGCCATGGAGTGGACTTAAATCACATTTATGGTGAAACTCTGG ACAGACAACATAAACTGCGCCTTTTCAAGGATGGAAAATTGAAATATCAGGTCATTGGTGGAGAGGTGTATCCCC CCACACCTCCCGCAGACCATGTTCCATGTTTCTTTTAGATATATCTTTGGAATTCCTCCACTGATCCTTGTTCTGCTG CCTGTCACATCATCTGAGTTTTCAGAATCTACCGACCATGGAGCGTGTGCTTGGCTTGTTGCTGTTGCTTCTGGTGC ACGCCTCTCCCGCCCCACCAGAGCCCTGCGAGCTAGACGAGGAAAGTTGTTCCTGCAACTTCTCAGATCCGAAGCC AGATTGGTCCAGCGCT
Actb	TGAAAAGATGACCCAGATCATGTTTGAGACCTTCAACACCCCAGCCATGTACGTAGCCATCCAGGCTGTGCTGTCG TTTCCTCGTCCCGTAGACAAAATGGTGAAGGTCGGTGTGAACGGATTTGGCCGTATTGGGCGCCTGGTCACCAGGA CTGCCAAGACTGAATGGCTGGATGGCAAGCATGTGGTCTTTGGGAAGGTGAAAGAAGGCATGAACATTGTGGAAG CCATGGAGCGTTTTGGGTCCAGGAATGGCAAGACCAGCAAGAAGATCACCATTTCCGACTGTGGACAGCTCTAAT TTCTTTTGACTTGCGGGCATTTT

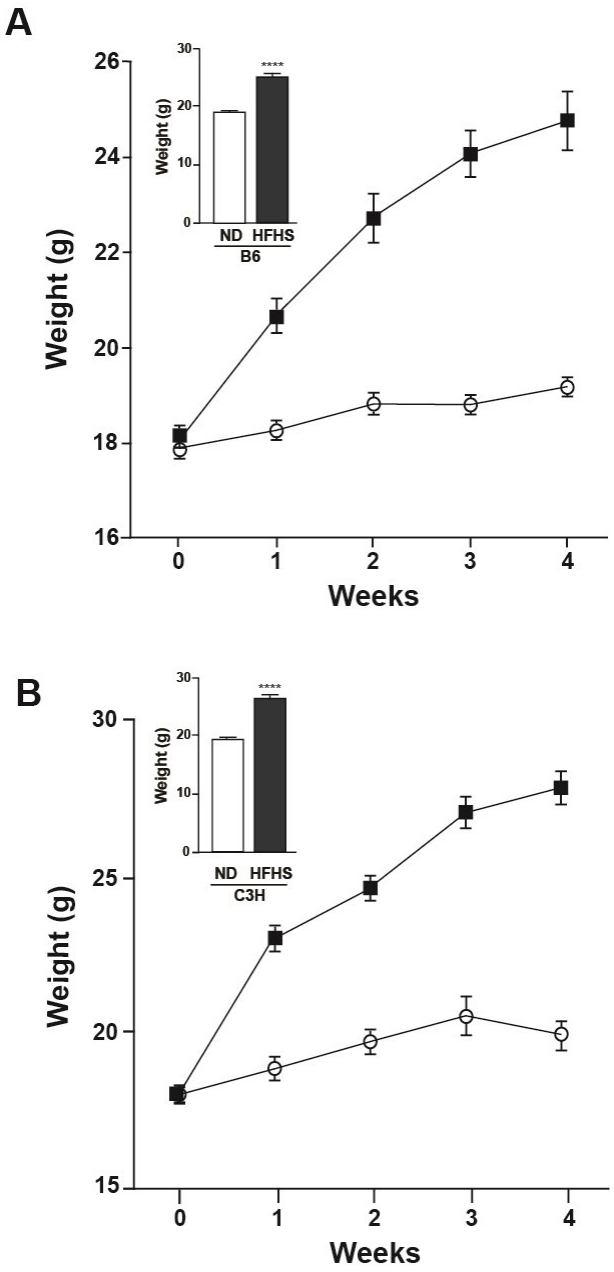

Supplemental FIgure 1.